J. Earth Syst. Sci. (2020)129 65
https://doi.org/10.1007/s12040-019-1300-9

Observational aspects of tropical mesoscale convective systems over southeast India

A Madhulatha[1,5,*], M Rajeevan[2], T S Mohan[3] and S B Thampi[4]

[1]*National Atmospheric Research Laboratory, Gadanki 517 502, India.*
[2]*Ministry of Earth Sciences, New Delhi, India.*
[3]*Khalifa University of Science and Technology, Abu Dhabi, United Arab Emirates.*
[4]*Doppler Weather Radar Division, India Meteorological Department, Chennai, India.*
[5]*Present address: Korea Institute of Atmospheric Prediction Systems, Seoul, South Korea.*
**Corresponding author. e-mail: madhulatha11@gmail.com*

MS received 17 April 2019; revised 31 August 2019; accepted 16 September 2019

To enhance the knowledge of various physical mechanisms related to the evolution of Tropical Mesoscale Convective Systems (MCSs), detailed analysis has been performed using suite of observations (weather radar, electric field mill, surface weather station, flux tower, microwave radiometer and wind profilers) available at Gadanki (13.5°N/79.2°E), located over southeast India. Analysis suggests that these systems developed in warm, moist environment associated with large scale low level convergence. Significant variations in cloud to ground (CG) lightning activity indicate the storm electrification. Deep (shallow) vertical extents with high (low) reflectivity and cloud liquid water; dominant upward (downward) motion reveals variant distribution in convective (stratiform) portions. Existence of both +CG and –CG flashes in convective regions, dominant –CG in stratiform regions explains the relation between lightning polarity and rain and cloud type. Sharp changes in surface meteorological variables and variations in surface fluxes are noticed in connection to cold pool of the system. Increase (decrease) in temperature, moisture and equivalent potential temperature (θe) within the boundary layer in convective (stratiform) regions associated with latent heat warming (cooling) of air parcel are apparent. Presence of updrafts and downdrafts in convective region and dominant downdrafts in stratiform regions are evident from vertical velocity measurements. Isentropic upgliding (downgliding) illustrate the existence of isentropic ascents (descent) of air parcels in the storm vicinity. Veering (backing) of wind due to warm (cold) and moist (dry) air advections demonstrated the formation of θe ridge in storm environment. Blend of observations provided considerable insight of electrical, microphysical, thermodynamic, dynamic and kinematic features of MCS.

Keywords. Mesoscale convective systems; cloud to ground lightning; isentropic sloping; wind profiler; microwave radiometer; doppler weather radar.

1. Introduction

Mesoscale convective systems (MCSs) are important links between convection and the large scale atmospheric circulation. MCS is defined as an ensemble of thunderstorms that produces a contiguous precipitation area of around 100 km or more in at least one direction (Houze 2004). These systems are characterized by regions of both convective and stratiform regions of precipitation.

Published online: 07 February 2020

Long-lasting, slow moving MCSs are major cause of flooding, and these systems often contain hail, strong winds, and lightning. Cloud to ground (CG) lightning associated with these systems can cause serious hazards to aviation and satellite launch operations. Understanding and predicting these severe convective systems is therefore of great socio-economic significance. Formation, intensification and propagation of MCS are mostly governed by synoptic and mesoscale conditions of the atmosphere (Johns and Doswell 1992). Important factors responsible for the formation of these systems include moisture supply, static stability, vertical motion and orographic effects (Doswell *et al.* 1996, 1998). Better understanding of these factors is important for improved weather forecasting of these severe convective systems (Weckwerth *et al.* 2008). Further, to investigate various mechanisms related to genesis of MCSs resulting from thermal and moisture advections, high resolution observations are necessary.

During the last few decades, considerable attention has been given to MCS by conducting various field campaigns, satellite measurements, and high resolution numerical simulations and by developing theoretical models. Role of observations and modeling efforts to understand and predict storm initiation, evolution, dynamics and scale interactions associated with the MCSs are discussed in review papers by Wilson *et al.* (1998), Houze (2004), and Moncrieff (2010). Considerable insight into the evolution of tropical MCS has been gained from various field experiments such as GATE (Global Atmospheric Research Program (GARP) Atlantic Tropical Experiment) (Houze and Betts 1981), TOGA/COARE (Tropical Ocean-Global Atmosphere/Coupled Ocean-Atmosphere Response Experiment) (Jorgensen *et al.* 1997), International H_2O Project (IHOP_2002) (Marsham *et al.* 2011), African Monsoon Multidisciplinary Analyses (AMMA) (Guy *et al.* 2011), Dynamics of the Madden–Jullian Oscillation (MJO)/Atmospheric Radiation Measurement (ARM) MJO Investigation Experiment (DYNAMO/AMIE) (Zuluaga and Houze 2013); (CINDY/DYNAMO) (Zhang and Yoneyama 2017), Tropical Warm Pool International Cloud Experiment (TWP-ICE)(Collis *et al.* 2013) and Large Scale Biosphere-Atmosphere (LBA) experiment (Laurent *et al.* 2002).

Other than campaign-based experiments, numerous diagnostic studies also been performed over different parts of the world by making use of various observations to characterize these convective systems (Wang 2004; Parker and Johnson 2004; Kim and Lee 2006; Ramis 2009; DeLonge *et al.* 2010; Lagouvardos *et al.* 2013; Helms and Harts 2015; Zhong *et al.* 2015). Key factors responsible for the formation of MCS around different parts of the globe include synoptic scale forcing mechanisms, topography, diurnal cycle of insolation and strong low level temperature and moisture advections (Mapes *et al.* 2003; Moore *et al.* 2003; Rasmussen and Houze 2011; Wapler and James 2015). Houze (1982) established that the life cycle of tropical MCS is characterized by convective towers in growth phase; convective and stratiform regions in mature phase and dominant stratiform regions in decay phase. Furthermore, the updrafts and downdrafts during different phases of convective system and the role of mesoscale downdrafts in the generation of convective updrafts along the gust front and its effect on longevity of MCS are well demonstrated by Rutledge *et al.* (1988). The conceptual model designed for tropical cloud clusters can be applied to mid-latitude convective systems; however, the systems vary in the horizontal arrangement of the convective and stratiform precipitation (Houze 1989). Kinematic structure of several tropical and mid-latitude MCS using wind profiler observations explained the dominant updraft (downdraft) cores in the convective (stratiform) regions (Cifelli and Rutledge 1998; Giangrande *et al.* 2013). Electrical structure from electric field mill observations reported dominant negative (positive) CG lightning flashes in convective (stratiform) components of mid-latitude and tropical MCSs (Rutledge and MacGorman 1988; Lang *et al.* 2004). Environmental characteristics using radiosonde observations revealed that the organization and development of tropical (Halverson *et al.* 2002) and warm season mid-latitude MCS (Moore *et al.* 2003) are aided by moderate to large Convective Available Potential Energy (CAPE), small Convective Inhibition (CIN) and moderate unidirectional low level wind shear. Significant variations in surface meteorological features are evident with the passage of gust front in the environment of tropical and mid-latitude MCSs (Houze 1979; Johnson and Hamilton 1988). And also, enhancement in sensible and latent heat fluxes associated with higher surface winds behind the leading edge of tropical MCS environment are reported by Johnson and Nicholls (1983). Furthermore, the thermodynamic structure of troposphere using continuous observations from

Microwave Radiometer (MWR) has provided the information of mesoscale phenomena over different regions in greater detail (Chan and Hon 2011; Cimini *et al.* 2011; Madhulatha *et al.* 2013; Ware *et al.* 2013). Using simultaneous wind profiler and radiometer observations, wind gusts associated with intense convective weather are also studied (Chan and Wong 2008). Research from many investigators emphasized the role of different observations in explaining various MCS features over different parts of globe.

On the other hand, in India, diagnostic studies have been carried out using individual observations to understand the tropical convective systems. For instance, surface meteorological parameters from the Automatic Weather Station (AWS) measurements have showed typical changes in surface features during the evolution of tropical convective system (Deshpande and Raj 2009; Rajeevan *et al.* 2010). Wind profiler and sound detection and ranging (SODAR) observations provided the evidence of largely varying vertical velocities representing the updrafts and downdrafts in the storm environment (Deshpande and Raj 2009; Latha and Murthy 2011). In a study by Mukhopadhyay *et al.* (2005) using Doppler Weather Radar (DWR) observations, different stages of severe storms formed over Kolkata (North east India) are studied. Further, few studies have been conducted to examine the structure and dynamics of severe convective systems over south east india using very high frequency (VHF) and ultra high frequency (UHF) wind profilers (Dhaka *et al.* 2002; Kishore Kumar *et al.* 2005; Abhilash *et al.* 2010). From these studies, it is inferred that most of the convective systems at this location are multi-cellular in nature. In addition, the importance of continuous monitoring of temperature and moisture profiles from MWR observations in storm environment is well demonstrated in Madhulatha *et al.* (2013, 2018).

Although few studies are made towards the understanding and prediction of these severe convective events, exhaustive studies are deficient mainly due to lack of mesoscale observational networks and modeling efforts (Das *et al.* 1999). Recently the Severe Thunderstorms – Observations & Regional Modeling (STORM) program has been carried out in India by the Department of Science and Technology (DST) which is a comprehensive observational study on the genesis, evolution and life cycle of tropical convective systems (Das *et al.* 2014). Using STORM experimental data various observational and numerical studies are carried out to understand basic characteristics of MCSs over northeast India (Abhilash *et al.* 2007, 2010; Joseph 2009; Litta *et al.* 2012). For example, based on electric field measurements, it is inferred that most systems in this region are associated with positive-dipole type charge structure (Gopalakrishnan *et al.* 2011). Similarly, flux tower measurements reported the variations in surface sensible and latent heat fluxes due to changes in surface temperature and moisture in the storm environment (Tyagi *et al.* 2012). Further, radiosonde observations have showed the presence of large amounts of moisture and convective instability present in the storm environment (Tyagi *et al.* 2013).

1.1 *Scope of the study*

Aforementioned studies are limited to characterize only certain features of MCS using fewer observations. Despite the knowledge on various MCS features, precise understanding of mesoscale processes is poorly documented, and no collective efforts have been made to understand the complex physical mechanisms and three dimensional structure of MCS over Indian region by making use of all available observations. Furthermore, several issues related to MCS remain unclear till date and there is still much to learn about complex physical mechanisms associated with these systems. Few important questions include:

What is the electrical evolution associated with lightning activity in a tropical MCS? Is there any relation between polarity of lightning flashes and microphysical, dynamic features of MCS? How do different meteorological parameters change in the storm environment? Does the association between dynamic and thermodynamic features affect temperature and moisture transport?

To address these issues, several parameters associated with the storm development needs to be monitored by making use of maximum number of collocated observations together. In order to understand the factors governing the evolution of these systems; high resolution observations of temperature, moisture, wind, precipitation, clouds and lightning are essential. For this purpose, a study region, National Atmospheric Research Laboratory (NARL), Gadanki (13.5°N/79.2°E) in southeast India has been selected in view of availability of many observational systems. A novel

feature of the present work is, the comprehensive analysis of MCS is performed using variety of observations including weather radar, lightning detector, MWR, wind profilers, AWS and flux tower to understand the underlying synoptic and complex mesoscale physical mechanisms responsible for the genesis, development and propagation of these severe convective systems for the first time. Combining the suite of observations can provide a detailed synthesis to investigate the physical processes associated with MCS evolution and their structure, and also interrelations between different physical processes. Current study thus provides a unique opportunity to analyze several aspects of MCSs over southeast India simultaneously.

The paper is organized as follows. Section 2 presents the description of study region followed by data and methodology in section 3. Results obtained from different meteorological observations are described in section 4. Conclusions are drawn in section 5.

2. Description of the study region

Present analysis is based on the observations made from a tropical site, NARL, Gadanki, a rural region situated in southeastern part of India. Height of the station is ∼370 m above mean sea level. It is a semi-arid region with annual rainfall of∼690 mm. The region is surrounded by hillock, whose heights are around 200–800 m, within 10 km radius. It is about 120 km to the northwest of Chennai city (13.0°N, 80.1°E), DWR site. Three-dimensional view of topography around Gadanki is shown in figure 1. It is a super observational site with variety of instruments, equipped with the state-of-the-art Indian Mesosphere–Stratosphere–Troposphere (MST) radar profiler operated at VHF range, UHF Lower atmosphere wind profiler (LAWP), AWS, and GPS balloon sonde. In addition to these observations, new suite of instruments like MWR, 10 m flux tower, and electric field mill (EFM) are installed in 2011 to understand the diurnal variation of severe convective systems.

3. Data and methodology

To examine the detailed structures of MCSs and to understand various underlying physical mechanisms, the convective systems for which most of observational data available are only considered. Life cycle, propagation and structure of MCS are investigated using DWR data obtained from India Meteorological Department (IMD), Chennai City, India. Infrared Brightness Temperature (Tb) from Kalpana-1 Geostationary satellite available from India Meteorological Department (IMD), Delhi is also used to understand the evolution of the system. The data is available at every 30 min with a spatial resolution of approximately 0.11° latitude × 0.11° longitude. Further details on the operational algorithm can be found in Thapliyal *et al.* (2011). Synoptic features responsible for the formation of MCS are studied using Modern-Era Retrospective analysis for Research and Applications (MERRA) data (Rienecker *et al.* 2011). Electrical evolution of the system has been examined using high frequency lightning observations from EFM. Frequency and location of the CG lightning flashes and their relation to the evolution

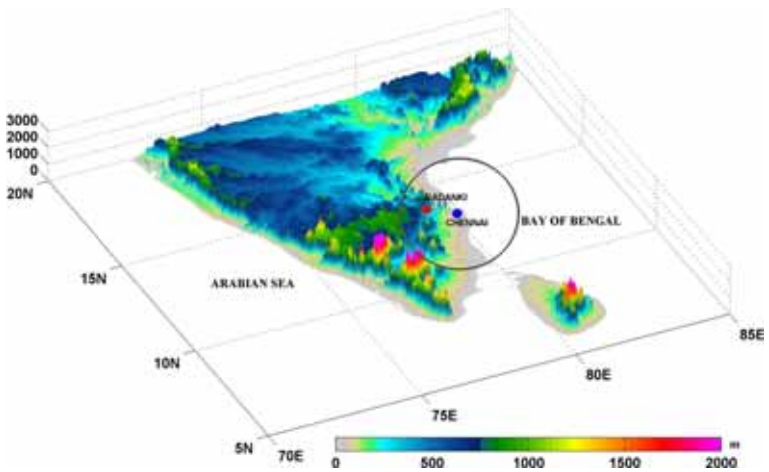

Figure 1. Areal view of the study region. Solid red circle represents observational site (Gadanki) and solid blue circle represents location of DWR (Chennai). Large grey open circle indicates DWR areal coverage.

of storm are studied using simultaneous DWR reflectivity and MWR liquid water content (LWC) measurements. Surface meteorological parameters (temperature, pressure, humidity, rainfall, wind speed and direction) during storm passage are analyzed using AWS and fluxes in the storm environment are studied from 10 m flux tower measurements. Thermodynamic stability and dynamical features are investigated utilizing high temporal measurements of temperature, moisture and wind from MWR and VHF/UHF wind profilers respectively.

A brief description of different observational platforms utilised is as follows. DWR is S-band (2875 MHz) radar with linear polarization and 1° beam width with klystron transmitter, solid state modulator and digital receiver. The effective range of these radars is $\sim$400 km and is based on Doppler principle to measure the target velocity. Scanning resolution is 10 min, with 1° azimuth and the base parameters available are reflectivity (Z), radial velocity (V) and spectral width (w). To visualize the weather systems using DWR, different scanning strategies are available. Plan position indicator (PPI) uses constant elevation angle to provide horizontal display whereas range height indicator (RHI) uses polar elevation scans at fixed azimuth angle to provide vertical cross section (Rajesh Rao *et al.* 2004). EFM manufactured by Vaisala is a real-time lightning system which monitors the development and dissipation of overhead lightning threats by measuring local atmospheric electric field within a range of $\pm$10,000 V/m, with an accuracy of $\pm$10%. More details can be found at (http://www.vaisala.com/en/products/thunderstormandlightningdetectionsystems/Pages/EFM550.aspx). MWR is a MP-3000A temperature, humidity and liquid profiler (manufactured by Radiometrics Corporation), operates in 21 K band (22–30 GHz) and 14 V band (51–184 GHz) microwave channels. It measures the radiation intensity of sky in 35 different channels both in oxygen and water vapour bands which are primary absorbers of atmospheric radiation. Retrieval of temperature and moisture profiles from the radiation intensity measurements is accomplished by neural network methods using historical radiosonde data. For the coefficient calibration of radiometer data, neural network algorithm has been trained using radiosonde data available at same location. MWR provides continuous profiles of temperature, relative humidity, water vapour and liquid water from surface to 10 km with temporal resolution of $\sim$5 min (Madhulatha *et al.* 2013; Ratnam *et al.* 2013).

Indian MST radar profiler is a pulse coded phase coherent Doppler radar operating at 53 MHz (VHF) frequency. It is a vertically pointing radar consists of 1024 crossed three elements Yagi-Uda antennas arranged in a 32 $\times$ 32 matrix covering an area of 130 m^2. Wind field is measured using Doppler Beam Swing (DBS) technique (Rao *et al.* 1995) which employs six beams (2 in zenith, 4 in off zenith) for obtaining winds at 4 min temporal and 150 m vertical resolutions. In general, MST radar profiler can provide both clear air and precipitation echoes due to Bragg and Rayleigh scatterings respectively. Turbulent irregularities in refractive index results in Bragg scattering whereas Rayleigh scattering arises from hydrometeors present in moderate to heavy precipitation (Carter *et al.* 1991). Doppler velocity spectrum during precipitation consists of two-well defined peaks in which the extreme downward velocity peak is from the hydrometeor reflectivity and non-zero spectral peak is from clear air radar return. Using adaptive spectral moment estimation technique, any non-zero Doppler shift interference and echoes have been eliminated (Anandan *et al.* 1996). In the current study only clear air MST radar profiler echoes are utilized.

LAWP is a coherent, phased array, Doppler radar operating at 1280 MHz (UHF) frequency. The phased array consists of 576 circular micro strip patch antenna elements arranged in a 16 $\times$ 16 matrix over an area of 3.8 m^2. It provides zonal, meridional and vertical wind components by using off zenith and zenith beams at 150 m range resolution respectively (Srinivasulu *et al.* 2012). For the present study we are mainly considering the precipitation echoes as LAWP is very sensitive to hydrometeors and receives strong backscatter from precipitation.

4. Results and discussion

Present study deals with two convective storms formed over southeast India on 1st June 2011 and 11th October 2011. To classify the convective systems, DWR reflectivity and rain rate observations are utilized. It is well noted from DWR observations that the spatial coverage of systems is greater than 100 km (figures 2 and 10) with life times more

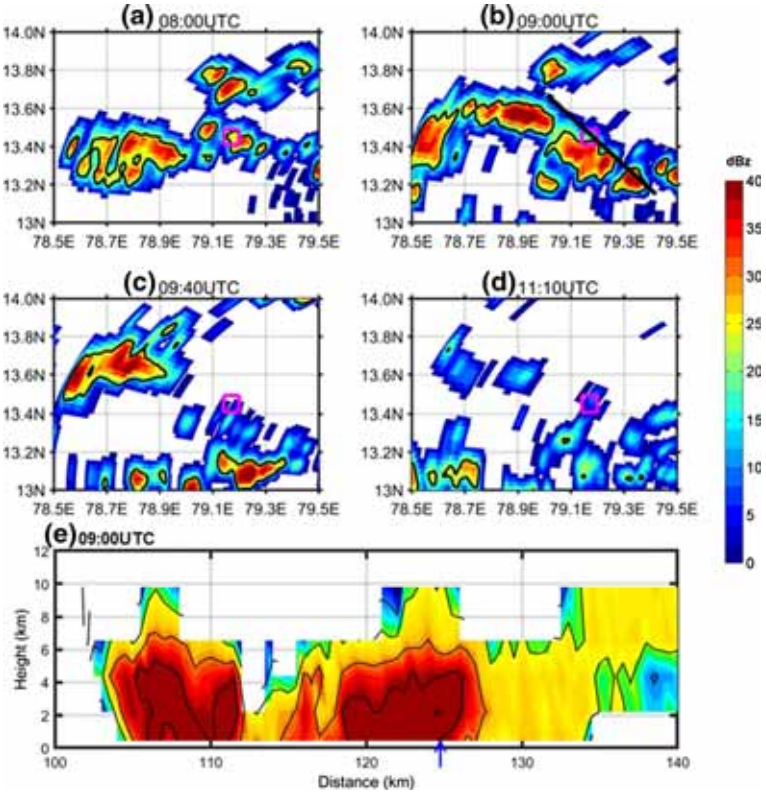

Figure 2. Spatial maps of DWR reflectivity (dBz) (shaded) and rain rate (mm/hr) (contours) associated with MCS on 1st June 2011 at various times. **(a)** 08:00 UTC, **(b)** 09:00 UTC, **(c)** 09:40 UTC, and **(d)** 11:10 UTC. Contour in figure 2(a–d) corresponds to 5 mm/hr rain rate. Open square in magenta denotes Gadanki and **(e)** space–height (x–z) cross section (along the solid black line in figure b) of DWR reflectivity at 09:00 UTC of 1st June 2011. Blue arrow indicates Gadanki.

than 6 hrs (figures 5 and 13). The considered systems are thus falling under MCS category as described by Houze (1989). Typically MCS are hundreds of kilometers in total horizontal dimensions and have lifetimes on the order of 10 hours and also important substructures such as convective cells and lines, gust fronts, meso lows and meso highs, tornadoes, etc., occur within the MCS on horizontal scales ranging from 1 to 50 km (Houze 1989). Also, using DWR derived reflectivity and rain rate observations, convective and stratiform regions of the systems are identified by following the criteria of Churchill and Houze (1984); Houze (1993). A region is classified as convective if its reflectivity is at least twice as large as the background reflectivity and more variable texture; and the regions which are not classified as convective and with more uniform texture are considered as stratiform (Churchill and Houze 1984). DWR rain rate values > 5 mm/hr are classified as convective and < 5 mm/hr are considered as stratiform regions (Houze 1993). System evolution and propagation characteristics are discussed in the following sections.

4.1 *Case 1: 1st June 2011*

4.1.1 *System evolution*

Spatial distribution of DWR reflectivity is used to examine the evolution and propagation of MCS formed over southeast India on 1st June 2011 and passed over Gadanki. Reflectivity maps (figure 2) shows a cluster of convective systems around 08:00 UTC surrounding Gadanki (magenta open square). Two major convective systems are visible, one over southeast and the other over southwest of the DWR site (13.0°N, 80.1°E). Initial movement of the system is from southwest of study region with a convective cell of reflectivity around 30 dBz (figure 2a). The system has further intensified and passed over Gadanki comprising of echo cells with peak reflectivity around 40 dBz representing convective portion and a relatively uniform area of stratiform precipitation with reflectivity values around 20 dBz (figure 2b). Later the system has moved north–northeast around 09:40 UTC (figure 2c) and a relatively weak convective cell with a reflectivity around 30 dBz is noticed

surrounded by stratiform precipitation regions. As the time progresses around 11:10 UTC, eastward propagation of MCS is observed (figure 2d) and stratiform region is more prominent. From the reflectivity and rain rate observations it is clear that the system has distributed to an area of nearly 1° (∼100 km) with multi-cell structure. Further, convective regions with relatively high reflectivity and rain rate values are surrounded by stratiform regions.

Space height cross section (x–z) of the convective system at 09:00 UTC is described in figure 2(e). It is noticed that the system has large spatial extent with several convective clusters and varying vertical extents with maximum height reaching up to 10 km. Over Gadanki, a convective cell with reflectivity (∼40 dBz) and vertical extent (∼10 km) is apparent (blue arrow in figure 2e). Large stratiform region of MCS is not clearly visible (figure 2e). This could be due to multi-cell nature of the systems. From DWR reflectivity maps, it is inferred that the system comprises of multiple cells with organized structure which indicates that the formation of MCS could have associated with large scale synoptic forcing which is discussed in the following section. Temporal evolution of infrared brightness temperature (Tb) from Kalpana-1 satellite observations shows the evolution, distribution and intensity of system. Infrared Tb values of less than 235 K are evident, associated with large convective regions surrounded by stratiform regions (> 235 K) of MCS (figure 3) as demonstrated by Yuter and Houze (1998). Eastward movement of the system is clearly evident.

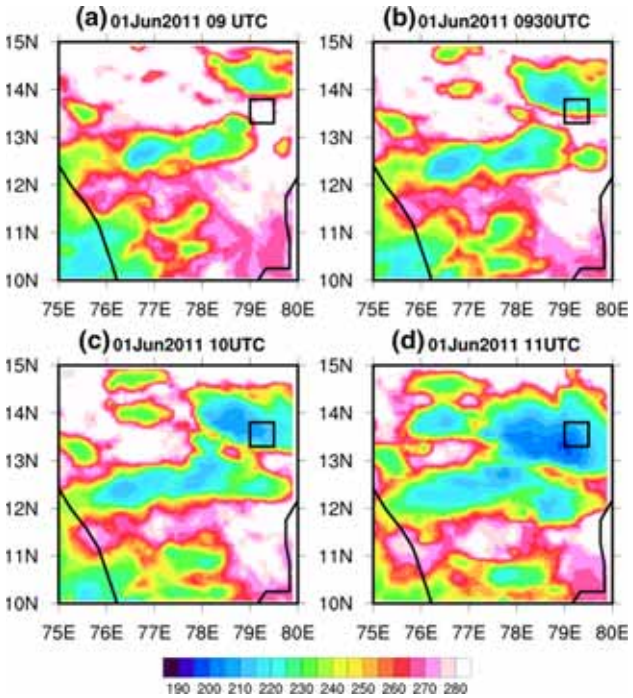

Figure 3. Spatial distribution of infrared brightness temperature (Tb) from IMD Kalpana satellite observations on 01June 2011 at various times **(a)** 09 UTC, **(b)** 0930UTC, **(c)** 10 UTC, and **(d)** 11 UTC. Open square in black represents Gadanki region.

4.1.2 *Prestorm meteorological environment*

Spatial distribution of mean sea level pressure (MSLP), winds and moisture at 850 hPa level using MERRA data during pre-environment of the storm are shown in figure 4. At 06:00 UTC, convergence associated with north–south trough is noticed over the study region, westerly winds are clearly seen (figure 4a). Relative humidity values of the order of 60% surrounding the study region (figure 4b) along with low level convergence are apparent (figure 4c). Synoptic scale convergence coupled with low level trough and large amounts of moisture in the surrounding regions might have created a favourable condition for the formation of MCS. Prior to the passage of MCS, the environment with large CAPE values of ∼1700 J kg^{-1} and low parcel inhibition energy CIN (–87 Jkg^{-1}) (figure 4d) depicts large potential for intense convective activity (Doswell *et al.* 1998). Lifting condensation level (LCL) and level of free convection (LFC) at lower levels, higher values of CAPE and various stability indices LI (–4.2°C), KI (∼40°C), TT (45.8) indicate conditionally unstable environment for the formation of severe convective system (figure 4d). Difference between temperature and dew point temperature profiles of around 2–3°C at lower levels indicate warm and moist environment prior to the system formation. Dominant westerly winds with magnitude of 5 knots are noticed below 800 hPa. Above this level, wind reversal is noticed and easterly winds of magnitude 10 knots are noticed around 550 hPa. Wind shear values of 5–10 knots are evident. Along with convective instability, presence of vertical wind shear can play important role in the sustenance of storm (figure 4).

4.1.3 *Life cycle of convective system over Gadanki*

Temporal evolution of convective system and related lightning, microphysical structure is studied using DWR reflectivity, EFM electric field intensity

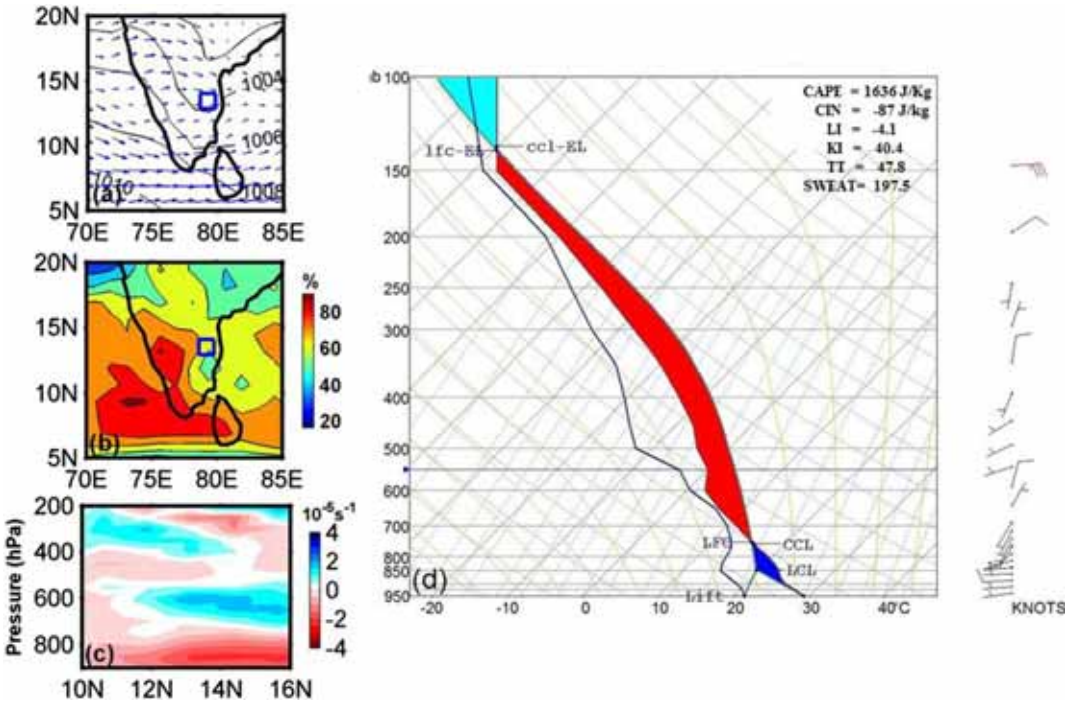

Figure 4. Spatial maps of different meteorological parameters **(a)** mean sea level pressure (MSLP) (contours) and wind vectors at 850 hPa, **(b)** relative humidity at 850 hPa (shaded), **(c)** space–height (x–z) plot of horizontal divergence ($\times 10^{-5}$/second, shaded) along 79.2°E, and **(d)** T–Ø diagram of temperature and dew point temperature profiles using MERRA data at 06:00 UTC of 1st June 2011 (blue open rectangle indicates study region).

and MWR derived LWC measurements respectively (figure 5). As discussed earlier, convective and stratiform regions of the system are classified using DWR observations and to support the classification, MWR derived LWC observations are utilized during the system passage overhead Gadanki region. Convective and stratiform portions of the system are indicated using DWR derived reflectivity and rain rate observations. Typical LWC values < 0.2 g/m^3 are classified as stratiform and > 0.2 g/m^3 as convective regions (Calhieros and Machado 2014). Time–height cross section of DWR derived reflectivity exhibits the passage of convective cell over Gadanki and it is noted that the system has sustained for long duration (∼6–7 hrs) (figure 5a). From reflectivity and LWC measurements, it is noticed that the passage of system shows the evidence of convective regions (08:00–10:00UTC) followed by stratiform regions (10:00–14:00 UTC). Further, rain rate values in convective regions are reaching up to 40 mm/hr (around 9:00 UTC); however, in stratiform regions rainfall <5 mm/hr are noticed (solid brown line in figure 5(a) corresponds to 5 mm/hr rain rate constant line).

Around 08:00 UTC, initial developing convective cell with reflectivity (∼40 dBz) (figure 5a), is observed associated with low-level convergence as noticed from low level winds (figure 4c). It has further intensified into strong convective cell with towers extending up to 11 km (∼08:30-09:00 UTC) with reflectivity (∼50 dBz) corresponding to mature phase of the storm. At 09:00 UTC surface AWS measurements (figure 6) showed the presence of cold pool of air related to precipitation (Byers and Braham 1949). Divergence associated with the cold pool interacts with low-level updrafts which can create negative feedback and decays the growth of convective cell (Houze *et al.* 1989). As a result, after 10:00 UTC convective cell started dissipating and stratiform regions with low reflectivity values (∼20 dBz) and more uniform texture are noticed. High/low reflectivity values are observed corresponding to convective/stratiform forms of precipitation.

Vertical motion in the respective regions is also studied using DWR derived vertical velocity (arrows in figure 5a). In convective regions dominant upward motion from surface to upper levels (∼8 km) represents the ascent of air parcel due to condensational heating. Also, convective downdrafts are mainly located around 4–5 km as a result of melting, precipitation loading and evaporation due to entrainment of dry environmental air.

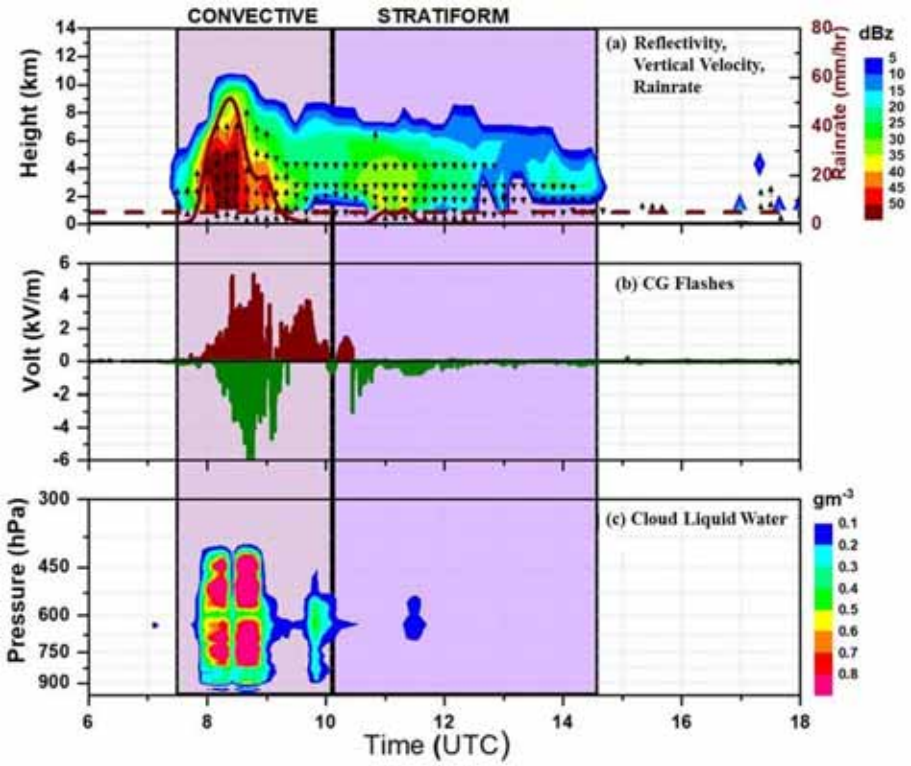

Figure 5. (**a**) Time height cross section of DWR reflectivity along with temporal evolution of DWR derived rain rate (solid brown line) and vertical velocity (arrows). **(b)** Temporal evolution of electric field intensity from EFM observations, and **(c)** liquid water content from MWR observations on 1st June 2011 over the study region (dashed brown line in (a) corresponds to 5 mm/hr rain rate constant line).

Presence of both updraft and downdraft motions represents mature phase of the system. In the stratiform regions, dominant downdraft motion is evident from middle (∼4 km) to lower levels. The vertical motion associated with the condensation and evaporation processes in convective and stratiform regions respectively explains the net heating of large scale environment (Houze 1982).

Cloud microphysical structure shows the evidence of strong convective cell (maximum LWC reaching up to 0.8 g/m^3) from 08:00–9:00 UTC and a weak convective cell (maximum LWC reaching up to 0.4 g/m^3) around 10:00 UTC (Figure 5c). High values of LWC (∼0.8 g/m^3) with clouds extending up to 400 hPa explain the presence of cumulonimbus clouds. Around 11:30 UTC, low values of LWC (<0.2 g/m^3) corresponding to stratiform portion of cloud are observed. Multi-cell structure of convective cell is apparent in MWR observations (figure 5c); however, it is not very clear in DWR (figure 5a). Also, DWR and EFM show stratiform region for longer duration compared to MWR. These discrepancies could be due to the differences in sampling strategies between the instruments. For instance, DWR measured reflectivity is based on volumetric scan and covers the storm activity near surroundings. Further EFM can provide the signature of storm activity within 30 km. However, MWR measures the convective activity overhead the study region.

EFM observations depict variability in the electric field intensity values due to CG lightning flashes related to the electrification processes. Large variations in CG flashes with values ranging between ±4 KV/m (figure 5b) are noticed. As lightning is manifestation of cumulonimbus cloud dynamics and microphysics (Peterson and Rutledge 1998), the relationship between the evolution of CG lightning flash and type of cloud is examined by considering convective/stratiform regions of the system. Both positive and negative CG strikes (+CGs and –CGs) are observed in the convective region (around 08:00–10:00 UTC) and negative CG flashes (–CGs) are dominant in the stratiform region (later 10:00 UTC) (figure 5b). Differential velocities between positive and negative particles cause collision breakup and results in movement of negative charge upward to smaller particles and positive charge resides on larger aggregates (Rutledge and MacGorman 1988) and contribute to polarity

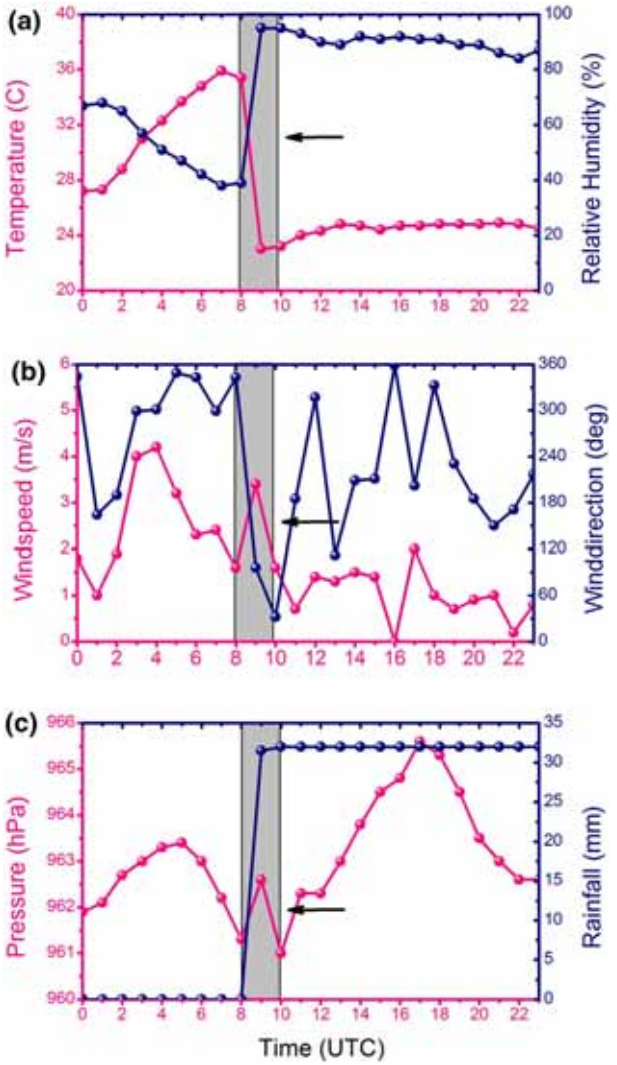

Figure 6. Evolution of surface meteorological parameters from AWS observations **(a)** temperature and relative humidity, **(b)** wind speed and direction, and **(c)** pressure and accumulated rainfall from AWS observations on 1st June 2011. Grey rectangle indicates storm passage.

differences in CG flashes in stratiform and convective portions. As reported in earlier studies, in the convective portions, the presence of cloud liquid water content of different sizes could have resulted in presence of both positive and negative flashes due to differential velocities of different size particles and associated collisions and in stratiform regions the negative charge could be due to uniform distribution of cloud liquid particles. However, the investigation of other hydrometeors is also important to understand the lightning polarity. Frequency of both +CG and –CG activity is highest around the most intense convective rainfall region (around 09:00 UTC) with high cloud liquid water content (figure 5c) and also frequency of –CG is more prominent in later stages of the storm (around 10:15 UTC). However, time lag is noticed between the peak negative and positive CG flashes and corresponding peak convective and stratiform activity as reported by Rutledge and Macgorman (1988). Correspondence between dominant –CG flashes (figure 5b) with stratiform region and both +CG and –CG flashes with convective region are also evident from MWR LWC observations (figure 5c).

4.1.4 *Surface meteorological variations*

Temporal evolution of surface characteristics of convective system is studied using hourly AWS observations (figure 6). Passage of the system is accompanied by sudden drop in temperature (cooling) by about 14°C and increase in relative humidity to 90% (figure 6a). Increase in wind speed and sudden change in wind direction is clearly noticed (figure 6b). Raise in surface pressure of the order of 2 hPa within 1 hr indicates 'meso high' associated with the cold pool of the storm and rainfall of about 30 mm is reported within 2 hr span (figure 6c). Even though the cold pool brings cold and dry air, the temperature drop could result in increase in relative humidity. These observed changes in surface parameters are due to the passage of cold pool ahead of storm as well as dry air accompanying the downdraft (Johnson and Hamilton 1988).

4.1.5 *Thermodynamic structure*

To obtain an insight of the air mass conditions in the storm environment, continuous profiles of temperature and moisture from MWR observations are examined. Time-height cross sections of temperature, vapour density, LWC and equivalent potential temperature (θe) up to 250 hPa are analyzed (figure 7). Associated with the storm, presence of cloud around 08:00–10:00 UTC is apparent in LWC observations with cloud base starting around 900 hPa (figure 7c). Large values of LWC ($\sim$0.8 g/m^3) around 08:00–10:00 UTC show the presence of deep clouds representing convective regions and relatively low values (0.2 g/m^3) during decay stage indicates stratiform portion (figure 7c).

In the pre-environment of the storm, large amounts of moisture, temperature and θe from surface to 900 hPa indicates the instability present in the atmosphere. In convective regions, increase in air temperature ($\geq$ 295 K) from surface to 700 hPa is noticed (figure 7a). This could be due to the latent

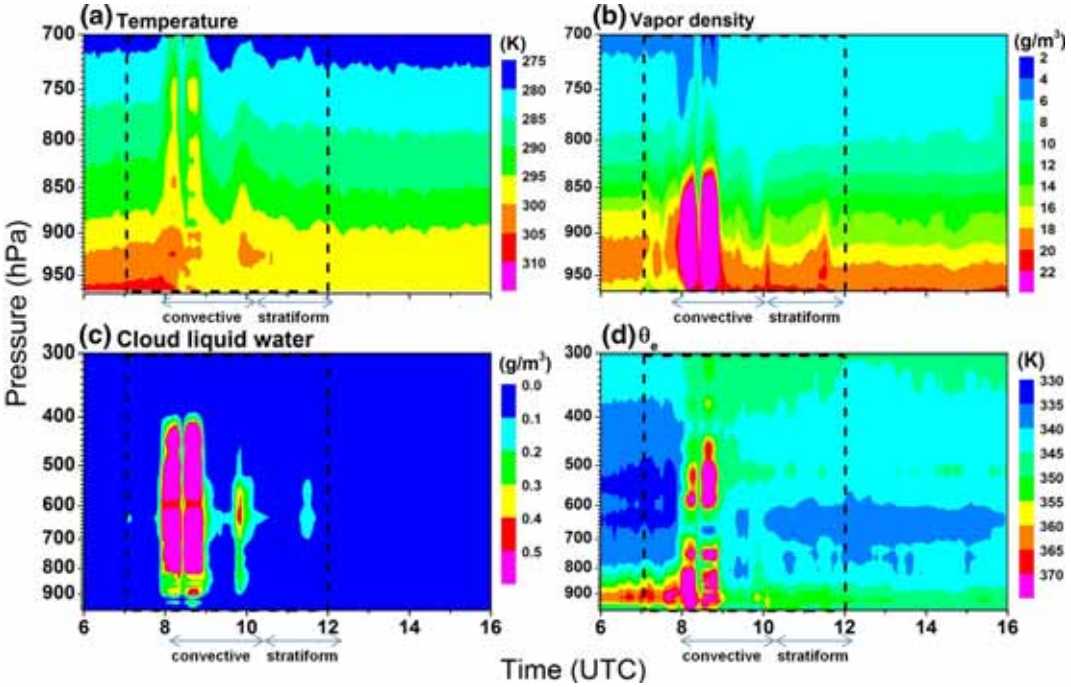

Figure 7. Time height cross section of MWR observed **(a)** temperature, **(b)** vapour density, (c) cloud liquid water, and (d) equivalent potential temperature on 1st June 2011(black dashed line represents the storm activity).

heat of condensation corresponding to the ascent of air parcel. Also raise in vapour density ($\geq$ 20 g/m^3) from surface to 850 hPa is observed (figure 7b) which explains the ascent of less dense buoyant moist air parcels resulted from surface warming (figure 7a). In the stratiform regions, decrease in these parameters demonstrates cold, dry descending air parcels due to latent heat of evapouration.

Large θ_e values ($\geq$360 K) at surface during pre-storm environment represent instability present in the atmosphere (figure 7d). Advection of temperature and moisture (figure 7a, b) below 850 hPa might have resulted in the formation of θ_e ridge around 08:00 UTC (reaching up to 500 hPa) which is considered as burst points for thunderstorms and severe convection. In convective regions, the variations in θ_e values are noticed from surface to 500 hPa (figure 7d) associated with variations in temperature and moisture at respective levels (figure 7a, b). In stratiform regions, decrease in θ_e with height (figure 7d) clearly indicates stable conditions due to latent heat of cooling related to evaporation and precipitation loading (figure 7a, b).

4.1.6 *Kinematic structure (convective updrafts/downdrafts)*

To investigate the kinematic structure of the convective system, different parameters derived from MST radar profiler are analyzed. Changes in signal-to-noise ratio (SNR) and vertical velocity associated with convective and stratiform regions are studied. In general, SNR is a function of refractive index fluctuations which depends on temperature, humidity variations in the atmosphere (Raghavan 2013). MST radar profiler data is available only for the period 08:30-10.30 UTC; therefore, we confined our discussion only to this time period (figure 8). White gaps in figure 8 indicate missing data. In convective region, SNR is distributed up to higher levels (around 14 km) indicating the mature stage of the system and in stratiform region it is confined only to lower levels ($<$9 km) representing dissipation (figure 8a). These changes in SNR are due to the variations in temperature and moisture fields in the storm environment as evidenced in MWR observations (figures 7a, b). Similar variations in SNR in the convective environment are also reported by Abhilash and Mohankumar (2009). In convective regions, vertical wind observations showed downdrafts of magnitude –2 ms^{-1} below 4 km (around 08:15 UTC) and updrafts (due to buoyancy) of magnitude 4 ms^{-1} above 6 km (figure 8b). During 08:45–09:15 UTC, updrafts of $\sim$5 ms^{-1} (around 8–14 km) coupled with middle level downdrafts of –2 to –5 ms^{-1} (around 5–8 km) are noticed in connection to the mature phase of storm. In the later stages between 10:00 and 10:30 UTC, below 6 km downdrafts are dominated due to stratiform precipitation.

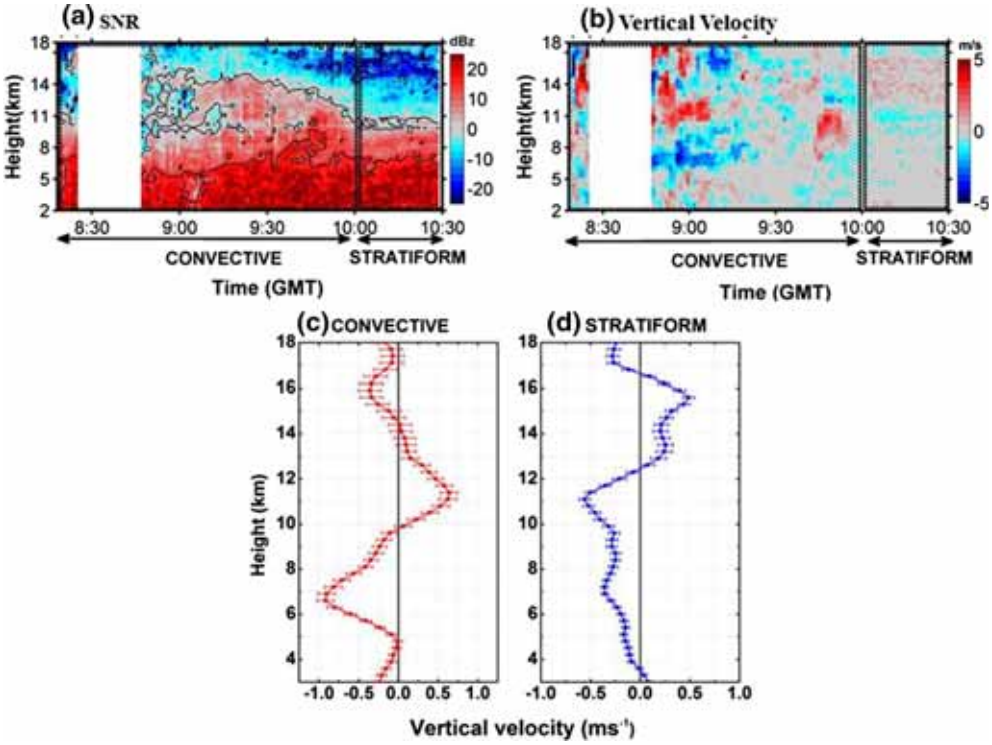

Figure 8. Time height cross section of MST radar derived **(a)** signal to noise ratio (SNR) in dBz, **(b)** vertical wind (m/s) and mean vertical velocity during **(c)** convective and **(d)** stratiform stages of MCS on 1st June 2011.

To understand the mean vertical motion associated with mesoscale flow, vertical velocity during convective and stratiform regions of MCS is averaged. Mean vertical motion in convective region exhibits dominant updrafts above 10 km and extending up to 14 km, with maximum values (around 0.5 m/s) at 11 km. Large amounts of latent heat released by freezing of super cooled water drops and vapour deposition growth of ice particles above freezing level might have contributed to cloud buoyancy and higher updraft speed in the middle and upper troposphere (Cotton and Anthes 1989). Below 10 km prominent downdraft motion is noticed and a maximum downdraft of about –1 m/s is observed around 7 km (figure 8c). Precipitation loading might have initiated downdrafts and then maintained by evaporation of cloud and precipitation (Johnson and Nicholls 1983). On the other hand, in stratiform region, downdrafts are prominent below 12 km with magnitudes up to –0.5 m/s (figure 8d). Latent heat of cooling related to melting might be the reason for driving negatively buoyant downdrafts (Leary and Houze 1979). From the analysis it is demonstrated that the mean vertical velocity patterns in convective region shows updraft/downdraft couplet representing the developing and mature phase of the system whereas stratiform region depicts dominant downdrafts related to dissipation. Similar patterns are reported by Houze (2004) and Abhilash and Mohankumar (2009). As the considered mesoscale convective systems are associated with large scale synoptic forcing, when the convective core passed over the study region it is already in the developing/mature stage, so the updraft and downdraft couplet structure is evident in the convective region.

4.1.7 *Thermodynamic/dynamic structure (isentropic lifting)*

To understand dynamical and thermodynamical structure of MCS, simultaneous observations available from MWR and MST radar profiler are utilised. As potential temperature (θ) is conserved quantity in adiabatic processes, it is used to study the displacements of isentropes which provide an estimate of the displacement of air parcel. Time height cross section of MWR derived θ along with MST radar profiler derived vertical winds during 08:00–10:55 UTC (480–650 min) of 1st June 2011 are shown in figure 9. In general, warm air advection results in sloping of isentropes upward (upgliding) and cold air advection results in descent (downgliding) of air parcel creating upward and downward motions respectively (Shaw and Austin 1930; Moore 1987). For instance, in convective region around

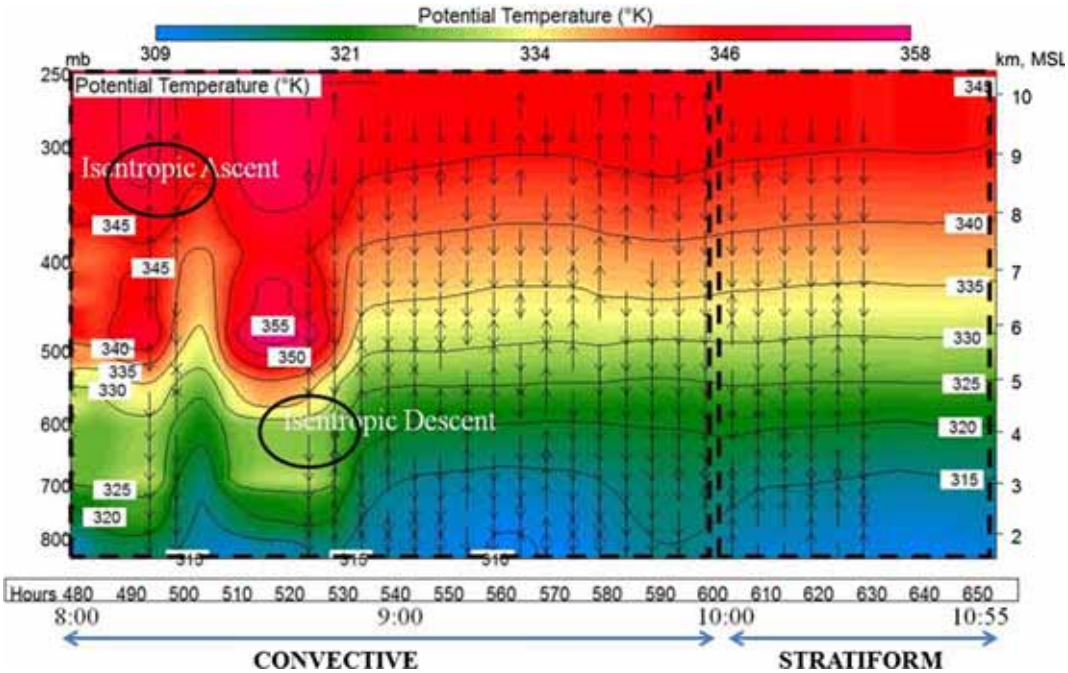

Figure 9. Time height cross section of MWR derived potential temperature (shaded) and MST radar derived vertical velocity (arrows) on 01st June 2011 (potential temperature is also plotted in contour for better visualisation). Black solid circles represent typical isentropic ascent and descent regions.

500 min, rise in θ surface (from ∼600 to 300 hPa) is observed (figure 9). This upward slope in isentropic surface might have resulted from warm air advection. Around 510 min, there is a downward slope in isentropic surface (from ∼500 to 600 hPa) which could be due to cold air advection. The sloping of isentropes is noticed from surface to higher levels (around 300 hPa) with respect to the air parcel motion. In convective region, the dominant isentropic ascent and descent are clearly evident representing the buoyant air parcels; however, in the stratiform regions (after 10:00 UTC) sloping is less due to stable conditions associated with subsidence. Rise (fall) in isentropes are nearly concurrent with upward (downward) motion of vertical velocity. Slope in isentropic surfaces from MWR observations are nearly simultaneous with MST radar profiler derived vertical wind (updrafts/downdrafts) measurements. Absence of vertical arrows in figure 9 corresponds to missing data from MST radar profiler.

4.2 *Case study-2: 11th October 2011*

4.2.1 *System evolution*

Spatial maps of DWR reflectivity on 11th October 2011 are shown in figure 10. An isolated system with reflectivity ∼40 dBz is observed around 07:53 UTC (figure 10a) and further intensified around 09:43 UTC during its passage over the study region (figure 10b). Large region of reflectivity values (>40 dBz) representing the convective portion surrounded by stratiform portions with reflectivity values (∼20 dBz) are clearly observed. Rain rate observations (contours in figure 10a–d) showed different distribution in convective and stratiform regions. System has extended spatially and oriented along the north-south direction. Around 10:23 UTC it has further moved to southeast direction and maintained intensity with stratiform region over Gadanki, representing dissipation of the system (figure 10c), later, it has moved away from Gadanki by 11:09 UTC (figure 10d). Space height cross-section of reflectivity at 09:43 UTC reveals that the system is well distributed with high vertical extent and large reflectivity values (figure 10e). Spatial distribution of system with ∼100 km and maximum vertical extent reaching up to 12 km is evident. Associated with this system, convective cell with reflectivity (∼40 dBz) and vertical extent (∼10 km) is observed over Gadanki region (blue arrow in figure 10e) and accompanying stratiform portion is also clearly noticed. Spatial and temporal distribution of the system with varied Tb distribution in convective and stratiform regions of MCS is also evident from Kalpana derived Tb observations (figure 11).

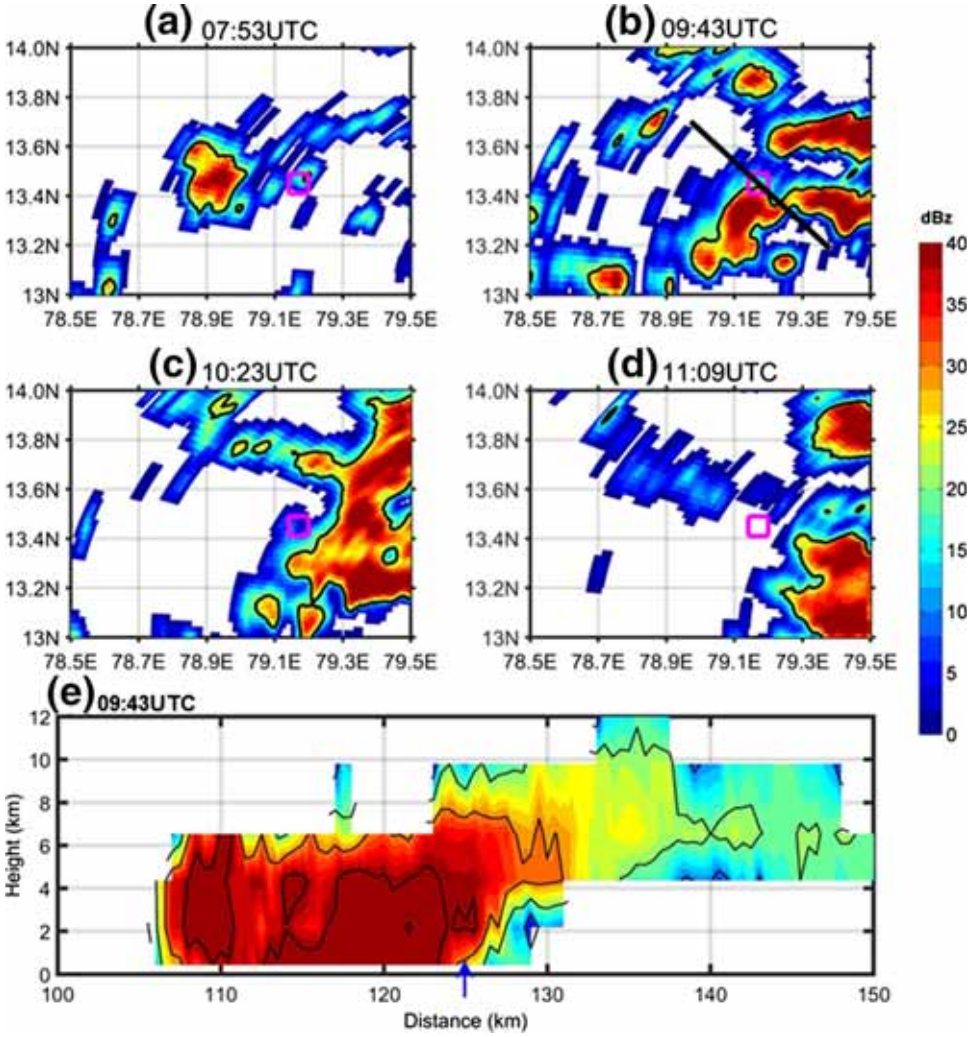

Figure 10. Spatial maps of DWR reflectivity (dBz) (shaded) and rain rate (mm/hr) (contours) associated with MCS on 11th October 2011 at various times **(a)** 07:53 UTC, **(b)** 09:43 UTC, **(c)** 10:23 UTC and **(d)** 11:09UTC. Contour in figure 10(a–d) corresponds to 5mm/hr rain rate. Open square in magenta denotes Gadanki, and **(e)** space–height (x–z) cross section (along the solid black line in figure 10b) of DWR reflectivity at 09:43 UTC of 11th October 2011. Blue arrow indicates Gadanki.

4.2.2 *Prestorm meteorological environment*

At 850 hPa, north-easterly and easterly winds are observed surrounding the study region around 06:00 UTC (figure 12a). Evidence of high relative humidity values (>80%) over the study region (blue rectangle in figure 12b) due to moisture transport by easterly and north-easterly winds from the adjoining Bay of Bengal is noticed (figure 12b). Low level convergence is clearly observed around 12–14°N (figure 12c). It is inferred that moist environments at low levels associated with convergence are responsible for the development of convective systems over the study region. Pre-environment thermodynamic sounding at 06:00 UTC shows LCL and LFC at lower levels indicating high potential for low level parcel acceleration, large values of CAPE (about 2346 Jkg^{-1}) and low CIN (about 5 Jkg^{-1}) indicate strong potential for the initiation of deep convection (figure 12d). Different stability indices LI (–4°C), KI (36°C) and TTI (45) specify conducive environment for storm development. Northeasterly winds at lower levels and easterly winds at different levels are noticed. Wind speed varies from 5 to 35 knots from surface to 150 hPa level. However, no wind reversal with height is noticed. Wind shear values ranging from 10–15 knots are evident in prestorm environment (figure 12d).

4.2.3 *Life cycle of convective system over Gadanki*

Corresponding to MCS formation on 11th October 2011, a convective system has passed over study

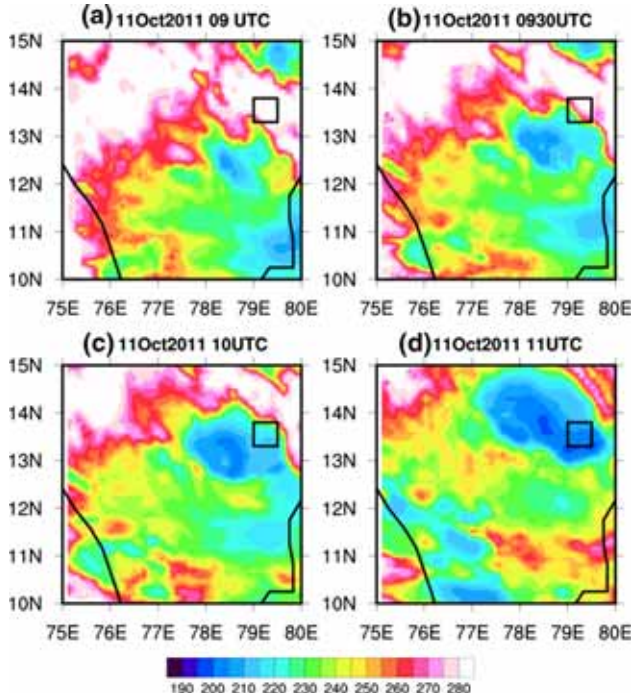

Figure 11. Spatial distribution of infrared brightness temperature (Tb) from IMD Kalpana satellite observations on 11 October 2011 at various times **(a)** 09 UTC, **(b)** 0930UTC, **(c)** 10 UTC and **(d)** 11 UTC. Open square in black represents Gadanki region.

region around 08:00 UTC and sustained till ∼11:20 UTC. Time–height cross section of DWR reflectivity is around 50 dBz with a vertical extent up to 10 km (figure 13a). A convective cell is observed around 09:00 UTC associated with the developing phase of system which has further intensified around 10:00 UTC and later dissipated. Convective and stratiform regions of MCS are apparent from reflectivity (figure 13a) and LWC measurements (figure 13c). From DWR derived vertical velocity it is inferred that in convective region, dominant updraft motion along with updraft/downdraft couplet corresponding to developing and mature phases of storm are noticed. Dominant downdraft motion in the lower levels accompanying the stratiform portion is also evident (arrows in figure 13a). And also, DWR measured rain rate shows intense rain (40 mm/hr) activity in convective regions followed by shallow precipitation (<5 mm/hr) in stratiform regions (solid brown line in figure 13a).

In addition, EFM measurements showed large variations in electric field intensity associated with CG lightning flashes. Frequency of both +CG and –CG activity is prominent in peak convective regions (around 10:00 UTC) and dominant –CG activity is seen in stratiform regions (around 12:00 UTC) (figure 13b).

4.2.4 *Surface meteorological variations*

AWS observations showed variations in basic surface meteorological parameters associated with the cold pool of system. Decrease in temperature by 8°C

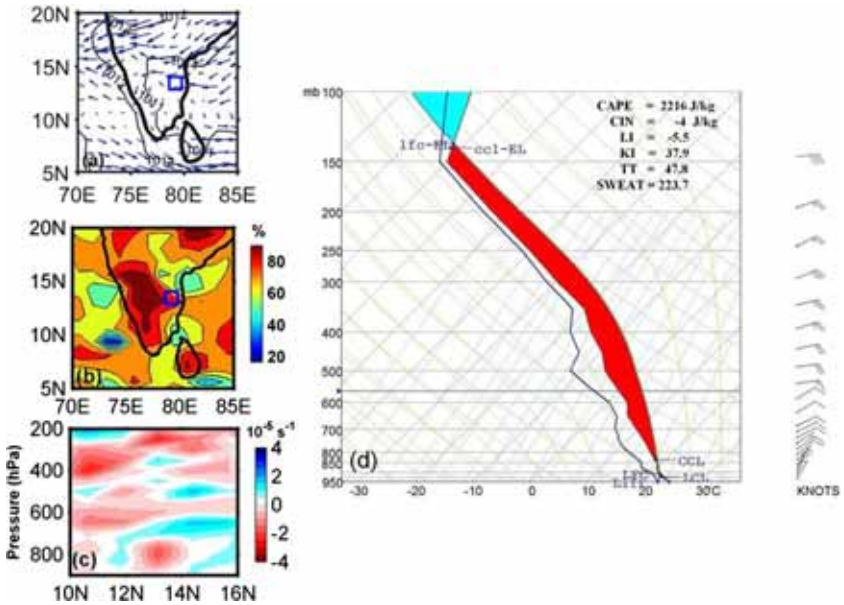

Figure 12. Spatial plots of different meteorological parameters **(a)** mean sea level pressure (MSLP) and wind vectors at 850 hPa, **(b)** relative humidity at 850 hPa, **(c)** space–height (x–z) plot of horizontal divergence ($\times 10^{-5}$/second, shaded) along 79.2°E and wind speed (ms^{-1}, contour), and **(d)** T–Ø diagram of the temperature and dew point temperature profiles using MERRA data at 06:00 UTC of 11th October 2011 (blue open rectangle indicates study region).

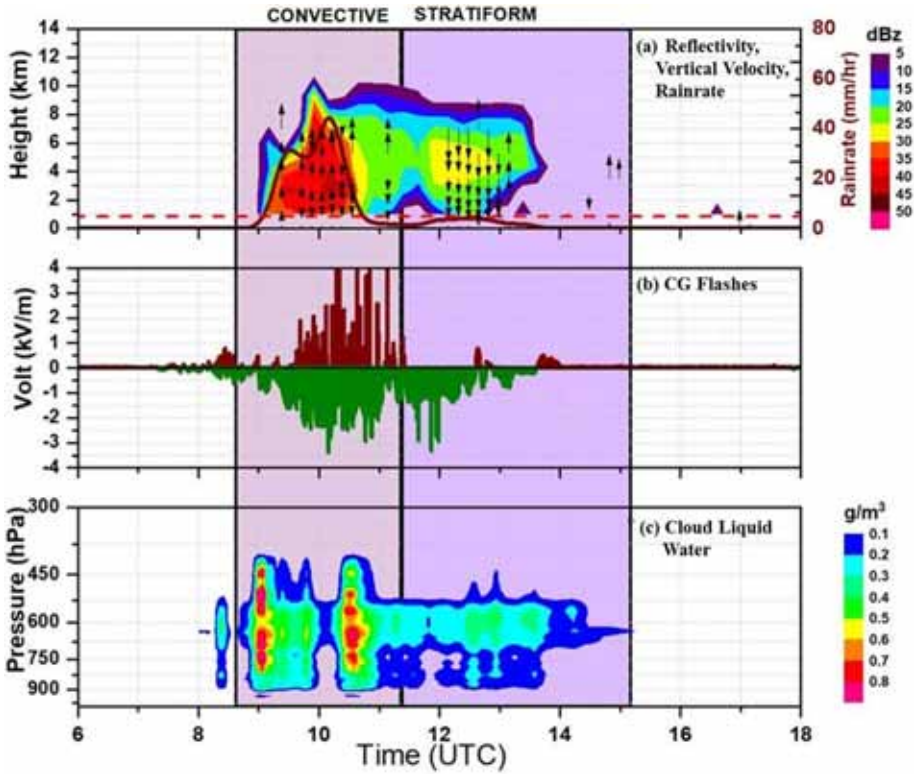

Figure 13. (**a**) Time height cross section of DWR Reflectivity; along with temporal evolution of DWR derived rain rate (solid brown line) and vertical velocity (arrows). **(b)** Temporal evolution of electric field intensity from EFM observations, and (c) liquid water content from MWR observations on 11th October 2011 over study region (dashed brown line in (a) corresponds to 5mm/hr rain rate constant line).

and increase in relative humidity by about 30%; sudden change in wind speed and wind direction; increase in pressure by 0.3 hPa and rainfall of about 50 mm are clearly observed (figure 14a, b and c). Variations in energy fluxes are also studied using flux tower measurements. This analysis is carried out only for the present case based on availability of data. To determine surface–atmosphere exchanges of energy, fluxes of sensible heat (SH) and latent heat (LH) are computed for 30 min period using eddy covariance methods (DeLonge *et al.* 2010). Rise in energy fluxes is reported around 07:00 UTC (figure 14d) due to increase in surface temperature and moisture in the pre-environment of storm (figure 14a). During the storm passage, modification of moisture and temperature along with strong winds generated by convective outflow contributes to variations in surface fluxes as reported by Jabouille *et al.* (1996). Further, gust front associated with downdrafts results in cooling, moisten and mix the boundary layer and reduce surface temperature and moisture gradients (Beringer and Tapper 2002). As a result, gradual decrease in magnitude of fluxes is noted following the storm decay.

4.2.5 *Thermodynamic structure*

Changes in temperature and moisture, during pre-storm environment, from surface to 700 hPa levels are clearly evident in MWR observations (figure 15). Maximum temperatures of $\sim$305 K, moisture $\geq$ 22 g/m^{-3} and $\theta_e \geq$ 360 K are observed respectively (figure 15a, b and d) around 08:00 UTC. In the storm environment, transport of temperature and moisture from surface to upper levels resulted in θ_e ridge (high values of θ_e) formation around 8:30 UTC extending up to 700 hPa. LWC values of $\sim$0.8 gm^{-3} and $\sim$0.2 gm^{-3} corresponding to convective and stratiform regions of the system are noticed (figure 15c). Gradual increase (decrease) in temperature, moisture and instability during convective (stratiform) portions of the system are clearly observed (figure 15).

4.2.6 *Kinematic structure (convective updrafts/downdrafts)*

During the convective phase (09.30–11:15 UTC), SNR is enhanced in the entire troposphere indicating developing to mature phase of the system.

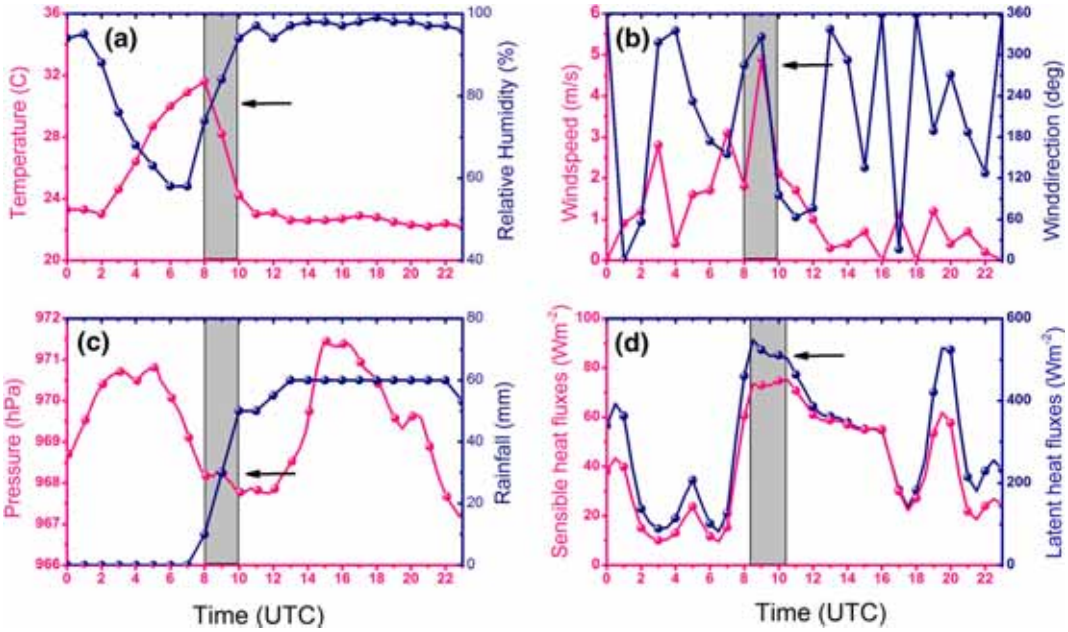

Figure 14. Evolution of surface meteorological parameters from AWS observations **(a)** temperature and relative humidity, **(b)** wind speed and direction, **(c)** pressure and accumulated rainfall on 11th October 2011, and **(d)** temporal evolution of surface sensible and latent heat fluxes from 10 m flux tower. Grey rectangle indicates storm passage.

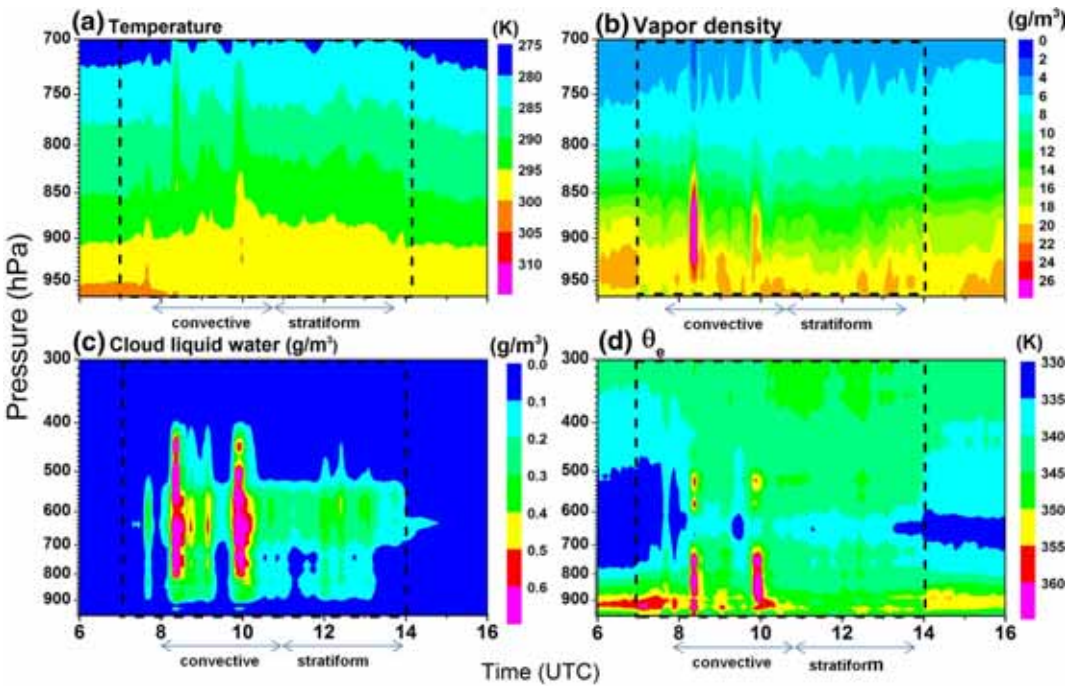

Figure 15. Time height cross section of MWR observed **(a)** temperature, **(b)** vapour density, **(c)** cloud liquid water, and **(d)** equivalent potential temperature on 11th October 2011 (black dashed line represents the storm activity).

However, in stratiform region (∼11:15 to 14:00 UTC), SNR magnitude is decreased and confined to lower troposphere representing the system decay (figure 16a). Time evolution of vertical velocities shows the maximum updrafts of magnitude 5 ms^{-1} around 10–12 km due to low level ascent associated with condensation/ freezing during developing and mature phases of the system. In the later stages, downdrafts of magnitude –2 to –4 ms^{-1} are dominant due to evapouration/precipitation loading during the dissipation of storm (figure 16b). Vertical motion averaged during convective and stratiform regions is presented in figure 16(c, d). In the convective regions, mean upward vertical motion is

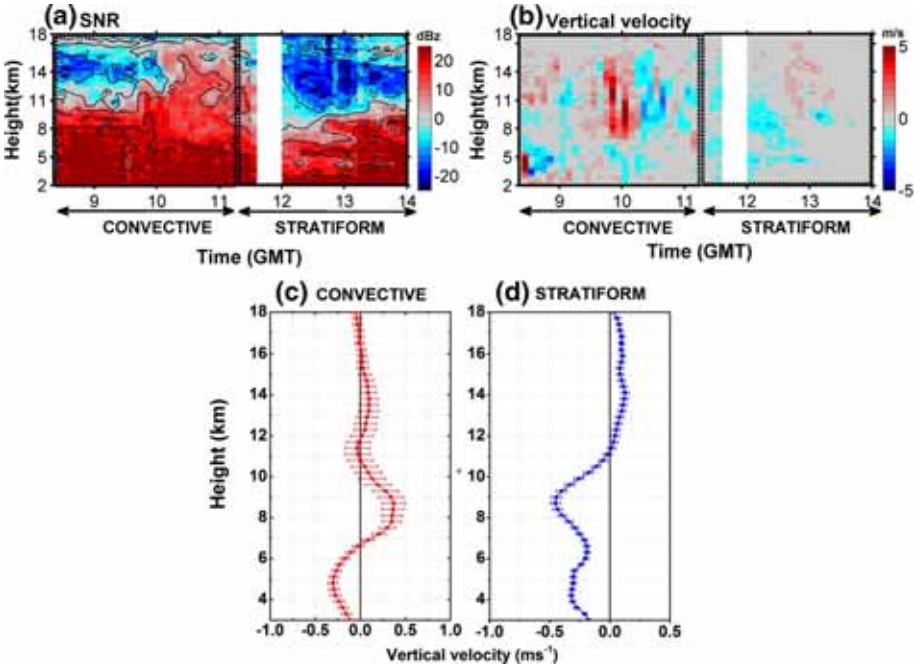

Figure 16. Time height cross section of MST radar derived **(a)** signal to noise ratio (SNR) in dBz, **(b)** vertical wind (m/s) and mean vertical velocity during **(c)** convective and **(d)** stratiform stages of MCS on 11th October 2011.

evident in the middle and upper levels (6–11 km) (figure 16c) and prominent downward motion is observed below 6 km. The coexistence of updraft and downdraft demonstrates mature phase of the storm. From the mean vertical velocity, it is evident that the updraft motion is dominant in middle and upper levels related with positive buoyancy and downdraft motion is prominent in the lower levels associated with precipitation. Maximum vertical winds of about 0.5 ms^{-1} are reported around 8 km. During decay phase, downdrafts are dominant from surface to upper levels (below 11 km) with maximum downdraft motion of greater than –0.5 ms^{-1} around 9 km (figure 16d).

4.2.7 *Thermodynamic/dynamic structure (isentropic lifting)*

MWR derived θ along with MST radar derived vertical winds during 08:00–14:00 UTC (480–840 min) of 11th October are shown in figure 17. In the convective region, around 495–510 min (08:15–08:30 UTC), upward sloping of isentropic surface of air parcel is clear from ∼800–750 hPa level and also downward sloping of isentropes is noticed around 585–600 min (09:45–10:00 UTC) from ∼750–800 hPa pressure levels (figure 17). The sloping of isentropes is observed up to 300 hPa. Clear evidence of upward (downward) displacement of air parcel and corresponding rise (fall) in isentropic surface is noted. As less dense warm air can lift over shallow surface of cold air, isentropic surfaces slope downward during cold air advection associated with downdraft and upward followed by warm air advection. In the convective region, presence of dominant isentropic ascent along with descent represents the vertical motion in developing and mature phases of the system. However, in the stratiform regions, dominant isentropic descent is noticed due to downdraft motion. Most of the isentropic ascents are nearly simultaneous with upward (updrafts) motion (vertical arrows in figure 17) and the isentropic descents (downdrafts) are simultaneous with the downward motion of air parcel. The differences between isentropic surfaces at different pressure levels are also highly pronounced during initial stages which correspond to most unstable atmospheres (gaps in vertical arrows corresponds to missing data from MST radar profiler).

Some discrepancies are observed between the association of vertical motion and isentropic sloping. For instance, around 500 min (08:20 UTC), large updrafts are noticed (∼800 to 500 hPa) however corresponding variations in isentropic surfaces are not very clear. As vertical motion of air parcel depends on many factors like diabatic heating rate, differences between isentropic

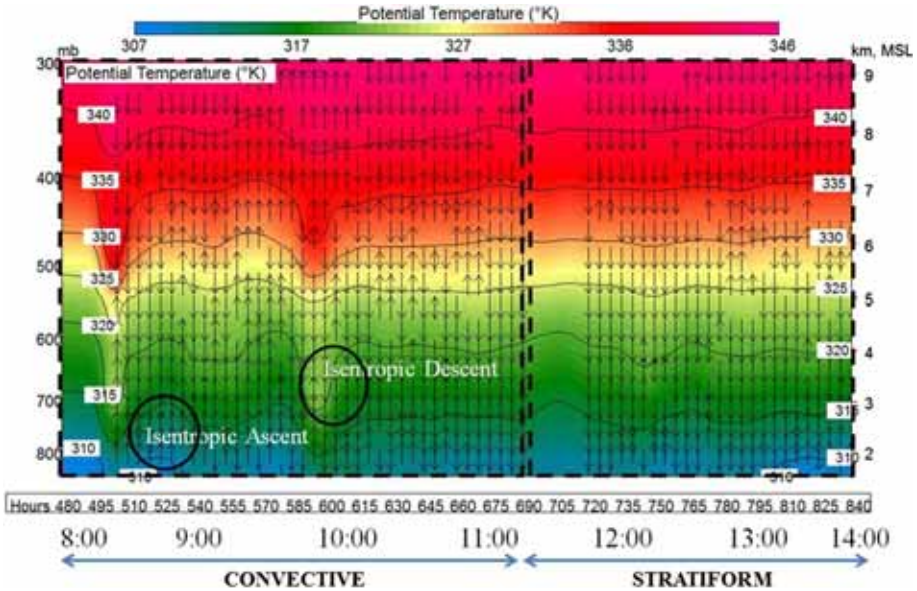

Figure 17. Time height cross sections of MWR derived potential temperature (shaded) and MST radar derived vertical velocity (arrows) on 11th October 2011 (potential temperature is also plotted in contour for better visualisation). Black solid circles represent typical isentropic ascent and descent regions.

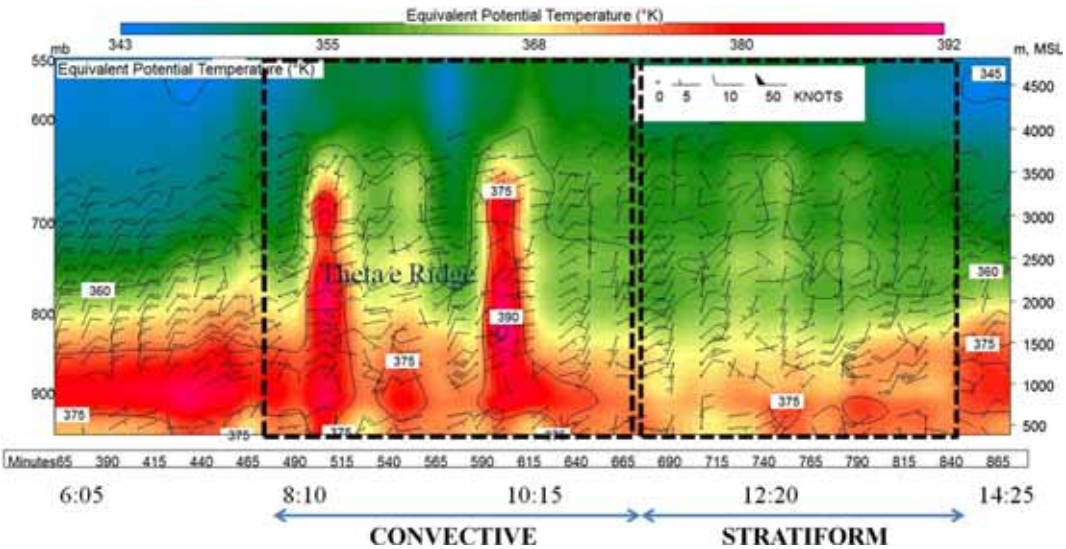

Figure 18. Time height cross section of MWR derived equivalent potential temperature superimposed with LAWP derived horizontal winds on 11th October 2011.

surfaces at different levels, pressure advection and background wind; the association between isentropic sloping and vertical air motions might be affected. Also, in the present analysis θ and vertical wind observations are from two different instruments which have different characteristics. Sampling errors of instruments can also affect the accuracy of measurements. Even with the limitations, the analysis of high-resolution UHF wind profiler and MWR observations has given considerable insight of isentropic sloping and vertical air motion.

4.2.8 *Dynamic conditions*

To examine the dynamical background wind structure along with thermodynamic features, horizontal winds from LAWP during 06:05–14:25 UTC (365–865 min) of 11th October 2011 are analyzed along with θ_e observations from MWR (figure 18). During convective activity strong variations in θ_e, wind speed and wind direction are noticed in the lower troposphere.

Prevailing north-easterlies which are prominent in the month of October are observed from surface to

600 hPa around 365 min (06:05 UTC) before the passage of storm. In the pre-environment of the storm around 465 min, easterlies at the surface are changed to westerlies around 850 hPa and again turned to north easterlies at 800 hPa and sustained as easterlies up to 600 hPa. Wind has turned in the clockwise direction from surface to 800 hPa resulted in veering in prestorm environment (Augustine and Zipser 1987). This veering of wind associated with warm air advection in convective regions is evident from MWR temperature and moisture profiles (figures 15a, b). This might have resulted in transport of warm moist air from surface to higher levels. Wind direction at the surface shifted abruptly from north easterlies to westerlies around 540 min (09:00 UTC) associated with cold pool evident from AWS observations (figure 14). Around 590 min, veering of wind is noticed again due to the variations in moisture and temperature. Along with change in wind direction, change in magnitude of wind is also evident which explains wind shear in the storm environment. And in later stages of storm, around 790 min surface westerlies changed to easterlies (around 800 hPa) indicating anticlockwise direction which represents backing of wind associated with cold air advection in stratiform regions. This analysis provides insight of dynamical response coupled with the thermodynamic variations at different layers of lower troposphere in the storm environment.

5. Conclusions

Detailed analysis of meteorological conditions associated with the passage of MCSs over southeast India using suite of observations is presented for the first time. Spatial maps of DWR reflectivity are utilized to identify the initiation, propagation characteristics and life cycle of two tropical MCS. Large scale flow patterns responsible for the formation mechanisms are studied from MERRA datasets. Temporal and vertical distribution of MCS and associated dynamical, lightning and microphysical structure are investigated by DWR, EFM and MWR measurements respectively. Surface features are analyzed using AWS and flux tower observations. Thermodynamic stability and kinematic features are inspected using MWR and UHF/VHF wind profilers. Vertical transports of temperature, moisture and winds are investigated by making use of MWR and wind profiler observations together. Several features of MCS are documented in greater detail and the key results of the present study are as follows.

Synoptic conditions during the prestorm environment using MERRA data reveal the presence of warm temperatures, high moisture and strong low-level convergence favourable for the formation of MCS. Pre-storm thermodynamic soundings showed large values of CAPE and high instability indices (LI, KI, TT) indicating strong potential for initiation of deep convection. DWR observations demonstrate that the passage of system is accompanied by convective regions with intense upward motion and towers extending up to higher levels indicating the developing phase and presence of upward/downward motion comprising of heavy precipitation representing the mature phase of the system followed by stratiform regions with prominent downdraft motion and less precipitation corresponding the decay phase. High values of reflectivity with deep vertical extents in convective regions and relatively low values with shallow vertical extents in stratiform regions reveals the varied vertical distributions of respective regions. Large (small) values of MWR derived LWC values represent the presence of deep (shallow) convective (stratiform) regions. EFM observations exhibit strong CG lightning activity with bipolar nature associated with the storm electrification processes. Simultaneous measurements of reflectivity, LWC and CG lightning are examined to understand the relationship between storm dynamics and lightning activity. The existence of both +CG and –CG flashes in convective regions and dominant –CG in stratiform regions shows the relationship between cloud type and lightning polarity. Presence of different size hydrometeors in convective regions could result in both positive and negative flashes due to collision between the different particles however in the stratiform regions the hydrometeor distribution is mostly uniform and could result only single polarity (negative flashes).

AWS observations reported the increase in surface temperature and moisture in the pre-storm environment responsible for storm initiation. Sudden change in surface parameters (temperature drop, gusty winds, reversal in wind direction, intense rainfall and meso high) indicates the cold pool of convective system. Strong enhancement in the surface energy fluxes are noticed from flux tower measurements representing the transport of heat, moisture and momentum in the boundary layer.

Thermodynamic structure in the storm environment governed by temperature and moisture advections in the troposphere is evident from MWR observations. High values of temperature, vapour density and θ_e from surface to boundary layer in the prestorm environment represents the strong instability. In the convective regions, increase in amplitudes of these parameters represents the warming and moistening of atmosphere due to latent heat of condensation. Decrease in amplitude corresponds to cooling associated with the latent heat of evapouration in stratiform regions. Kinematic features from MST radar profiler observations showed significant variations in SNR and vertical wind. In convective regions, SNR is distributed to higher levels however it is confined to lower levels in the stratiform regions. These changes can be attributed to variations in temperature and moisture distributions in respective regions which can alter the parcel buoyancy and determine the ascent/descent of air parcel. Mean vertical velocity in convective regions showed dominant updrafts with updraft/downdraft couplet related to developing and mature phase of the system followed by dominant downdrafts in the stratiform regions.

To understand the dynamic response in connection to thermodynamic variations, MWR and MST/LAWP derived vertical winds are analysed together. Isentropic analysis is carried out to get insight of three-dimensional transports of temperature and moisture. Interestingly, association between isentropic sloping and variations in vertical motion of air parcel are clearly apparent from this analysis. Isentropic upgliding (downgliding) is associated with ascent (descent) of air parcel. In the convective regions, strong isentropic upgliding (ascent) suggests the transfer of momentum to higher levels by ascending air parcel and dominant downgliding in the stratiform regions corresponds to descending air parcel. Dynamic structure of horizontal winds and transport of temperature and moisture are studied using LAWP derived winds and MWR observations. Strong variations in wind speed and direction are observed explaining the wind shear in the storm environment. In the convective regions strong veering of wind due to warm air advection is apparent and backing of wind associated with cold air advection is prominent in stratiform regions. Thermodynamic and dynamic structure of the troposphere resulting from thermal and moisture advection and three-dimensional wind fields explained the formation of θ_e ridge in the storm environment.

The present work thus provides unique opportunity to understand various physical mechanisms associated with the MCS. Several features of tropical MCS are documented in greater detail and the present results are corroborating with the earlier campaign-based observations. For instance, similar types of synoptic conditions are associated with the tropical MCS formed over other regions (Halverson *et al.* 2002; Zuluaga and Houze 2013). Convective and stratiform regions associated with MCS structure are also reported by Houze and Chang (1977). Present analysis shows the existence of both positive and negative CG flashes in the convective region and dominant negative CG in stratiform region which are different from the earlier studies by Rutledge and MacGorman (1988) who reported the presence of dominant negative CG in convective regions and positive CG flashes in stratiform regions. Also, the typical bright band structure associated with the MCS over the mid-latitude regions are not noticed in the current considered tropical MCS. These differences in microphysical structure can affect the lightning polarity. Variations in surface meteorological parameters in response to passage of gust front are in agreement with Weckwerth *et al.* (2008). Similar enhancement in surface energy fluxes during storm passage in connection with surface variations in temperature and moisture are investigated by Parsons *et al.* (1994). Further the thermodynamic structure associated with temperature and moisture advections in the storm environment are consistent with Knupp *et al.* (2009). The existence of updraft and downdrafts related to kinematic structure of storm are also reported by Collis *et al.* (2013). The veering of wind in the storm environment is also suggested by Augustine and Zipser (1987).

It is important to note that the present results demonstrated various features of tropical MCS which are in agreement with existing literature and also investigated several new findings related to MCS over southeast India. To our knowledge this paper provides the first detailed study on thermodynamic, dynamic, kinematic, microphysical, electrical structure and life cycle of tropical MCS using suite of observations. Combination of different observations has provided the opportunity to examine the interrelations of different physical mechanisms in the storm environment. Inspection of reflectivity, CG lightning and cloud liquid water

measurements have demonstrated the relationship between lightning with storm dynamics and cloud microphysics. Continuous profiles of temperature, moisture and wind measurements have given considerable insight of θ_e ridge formations associated with temperature and moisture advections. Isentropic upgliding and downgliding facilitated the unique way to visualise the vertical transport of temperature and moisture through ascent and descent of air parcel. Blend of different observations presented considerable insight of synoptic and complex mesoscale processes and their mutual interactions in the storm environment and provided encouraging results in explaining the three-dimensional structure of MCS over southeast India. However, the present study has certain limitations.

Two case studies with limited data leaves several important questions unanswered. The mechanisms responsible for association between CG polarity and convective/stratiform regions are not clearly stated. In this study the relation between lightning polarity in convective and stratiform regions are studied based on rain type and cloud liquid water; however, the effect of other hydrometeors needs to be studied. Therefore, there is a need for more comprehensive measurements (viz., polarimetric radar) in order to precisely define the convective and stratiform regions of tropical MCS and to understand the relationship between cloud microphysics and cloud electrification processes. Also, the present analysis is based on only observations available at Gadanki grid point; however, to get more insight of mesoscale circulations responsible for evolution of MCS there is a need of meso observation network (Rajeevan *et al.* 2010). Further, flux tower and LAWP observations are available only for one case and also data gaps are present in LAWP observations; all these factors limit the understanding of various physical processes. To get more insight of these systems, analysis of continuous observations is necessary. In explaining various features of MCS, discrepancies may also arise from differences in estimates of several observations, analysis methods or sampling strategies. Further, instrumental biases can also affect the accuracy of various observations. For instance, numerous considerations of DWR like ground clutter, anomalous propagation, and bright bands (Hubbert *et al.* 2009) can cause errors in measurements. VHF wind profiler observations during precipitation can result in the downward bias in Doppler spectra due to contamination from downfalling hydrometeors even after applying the filtering techniques (Williams 2012). Also, instrument biases of MWR measurements can contribute to inaccurate representation of temperature and moisture profiles (Madhulatha *et al.* 2013).

Furthermore, analysis of significant number of additional cases are required to determine whether the conclusions drawn based on the present study are representative of convective systems over other regions. To better characterise and quantify the differences between features associated with the tropical MCS and other regions, future research will focus on statistical analysis of large number of convective systems over southeast India. And also, additional analyses with wide range of observations will help to examine the complex convective scale processes associated with these systems. A convective scale resolving numerical model simulation has to be carried out to validate the hypothesis obtained from different observations. Even with certain constraints, the present study highlights the importance of observations in understanding various physical mechanisms responsible for the formation of severe storms. Improved understanding of different synoptic and mesoscale processes responsible for the severe convection will further improve the forecast. Importance of observations in evaluating the performance of various parameterisation schemes in simulation of MCS is well documented in Madhulatha and Rajeevan (2018). Assimilation of all these observations can provide convective scale information into mesoscale model's initial conditions (Madhulatha *et al.* 2017, 2018) which can improve the forecast of these severe weather systems. Overall, present work highlights the importance of observations to better understand the complex mesoscale processes.

Acknowledgements

This research was funded by National Atmospheric Research Laboratory (NARL) under the Junior Research Fellowship (JRF) program sponsored by Department of Space (DOS), India. The first author was funded to carry out her PhD work under this program. Authors gratefully acknowledge Director, NARL for his support and encouragement in providing necessary facilities and observations to carry out this work. The *in-situ* observational datasets utilized in the present study can be accessed by filling the data request form

under data dissemination tab and data services (available data) at https://www.narl.gov.in/. The DWR data can be obtained by requesting Deputy Director General of Meteorology, India Meteorological Department (IMD), Chennai (http://www.imdchennai.gov.in/). Special thanks to technical staff of Doppler Weather Radar Division, IMD, Chennai, India for their support in archiving the DWR data. NASA Goddard Earth Science Data and Information Services Centre is acknowledged for providing MERRA data (http://disc.sci.gsfc.nasa.gov/daac-bin/DataHoldings. pl). We would like to thank Dr. Ashim Kumar Mitra, India Meteorological Department (IMD), Delhi for retrieving the Kalpana Satellite Data. We also like to thank the anonymous reviewers for their constructive reviews which helped us to improve the quality of the manuscript.

References

Abhilash S, Das S, Kalsi S R, Gupta M D, Kumar K M, George J P, Banerjee S K, Thampi S B and Pradhan D 2007 Assimilation of Doppler Weather Radar observations in the mesoscale model for the prediction of intense rainfall events associated with mesoscale convective systems using 3DVAR; *J. Earth Syst. Sci.* **116** 275–304.

Abhilash S and Mohankumar K 2009 Vertical structure and evolution of a supercell storm: Observations using VHF radar; *Int. J. Remote Sens.* **30** 1441–1454.

Abhilash S, Mohankumar K, Das S and Kishore Kumar K 2010 Vertical structure of tropical mesoscale convective systems: Observations using VHF radar and cloud resolving model simulations; *Meteorol. Atmos. Phys.* **109** 73–90.

Anandan V K, Balmuralidhar P, Rao P B and Jain A R 1996 A method for adaptive moments estimation technique applied to MST radar echoes. *Progress in electromagnetic research symposium. Telecommunication Research Center*, City University of Hong Kong.

Augustine J A and Zipser E J 1987 The use of wind profilers in a mesoscale experiment; *Bull. Am. Meteor. Soc.* **68** 4–17.

Beringer J and Tapper N 2002 Surface energy exchanges and interactions with thunderstorms during the Maritime Continent Thunderstorm Experiment (MCTEX); *J. Geophys. Res.* **4552** 107(D21), https://doi.org/10.1029/2001jd001431.

Byers H R and Braham R R 1949 The thunderstorm: Report of the Thunderstorm Project, US Government Printing Office.

Carter D A, Ecklund W L, Mcafee J R, Gage K S, Keenan T and Manton M 1991 Results from the first year of observations using the Darwin VHF wind profiler; Preprints. 25th International Conference on Radar Meteorology, Paris, France (Boston: American Meteorological Society), pp. 288–291.

Calhieros A P J and Machado L A T 2014 Cloud and rain liquid water statistics in the CHUVA campaign; *Atmos. Res.* **144** 126–140.

Chan P W and Wong K H 2008 Application of microwave radiometer and wind profiler data in the estimation of wind gust associated with intense convective weather; Proceedings of the IOP Conference Series: Earth and Environmental Science.

Chan PW and Hon K K 2011 Application of ground-based, multichannel microwave radiometer in the nowcasting of intense convective weather through instability indices of the atmosphere; *Meteorol. Z.* **20** 431–440.

Churchill D D and Houze Jr R A 1984 Development and structure of winter monsoon cloud clusters on 10 December 1978; *J. Atmos. Sci.* **41** 933–960.

Cifelli R and Rutledge S A 1998 Vertical motion, diabatic heating, and rainfall characteristics in north Australia convective systems; *Quart. J. Roy. Meteorol. Soc.* **124** 1133–1162.

Cimini D, Campos E, Ware R, Albers S, Graziano G, Oreamuno J, Joe P, Koch S, Cober S and Westwater E 2011 Thermodynamic atmospheric profiling during the 2010 Winter Olympics using ground-based microwave radiometry; *IEEE Trans. Geosci. Remote. Sens.* **49** 4959–4969.

Collis S, Protat A, May P T and Williams C 2013 Statistics of storm updraft velocities from TWP-ICE including verification with profiling measurements; *J. Appl. Meteor. Climatol.* **52** 1909–1922.

Cotton W R and Anthes R A 1989 *Storm and cloud dynamics*; Academic Press, Oxford, 280p.

Das S, Daniel Johnson and Tao W K 1999 Single-column and cloud ensemble model simulations of TOGA-COARE convective systems; *J. Meteor. Soc. Japan* **77** 803–826.

Das S, Mohanty U C, Ajit Tyagi, Sikka D R, Joseph P V, Rathore L S, Arjumand Habib, Saraju K B, Kinzang Sonam and Abhijit Sarkar 2014 The SAARC STORM: A coordinated field experiment on severe thunderstorm observations and regional modeling over the South Asian Region; *Bull. Am. Meteorol. Soc.* **95** 603–617.

DeLonge M S, Fuentes J D, Chan S, Kucera P A, Joseph E, Gaye A T and Daouda B 2010 Attributes of mesoscale convective systems at the land-ocean transition in Senegal during NASA African monsoon multidisciplinary analyses; *J. Geophys. Res.* **115** P.D10213, https://doi.org/10.1029/2009jd012518.

Deshpande S M and Raj P E 2009 UHF wind profiler observations during a tropical pre-monsoon thunderstorm – case study; *Atmos. Res.* **93** 179–187.

Dhaka S K, Choudhary R K, Malik S, Shibagaki Y, Yamanaka M D and Fukao S 2002 Observable signatures of a convectively generated wave field over the tropics using Indian MST radar at Gadanki (13.5 N, 79.2 E); *Geophys. Res. Lett.* **2918** 1872–1879.

Doswell III C A, Brooks H E and Maddox R A 1996 Flash flood forecasting: An ingredient-based methodology; *Wea. Forecasting* **11** 560–581.

Doswell III C A, Ramis C, Romero R and Alonso S 1998 A diagnostic study of three heavy precipitation episodes in the western Mediterranean region; *Wea. Forecasting* **13** 102–124.

Giangrande S E, Collis S, Straka J, Protat A, Williams C and Krueger S 2013a A summary of convective-core vertical velocity properties using ARM UHF wind profilers in Oklahoma; *J. Appl. Meteor. Climatol.* **52** 2278–2295, https://doi.org/10.1175/jamc-d-12-0185.1.

Gopalakrishnan V, Pawar S D, Murugavel P and Johare K P 2011 Electrical characteristics of thunderstorms in the eastern part of India; *J. Atmos. Sol.-Terr. Phys.* **73** 1876–1882, https://doi.org/10.1016/j.jastp.2011.04.022.

Guy N, Rutledge S A and Cifelli R 2011 Radar characteristics of continental, coastal, and maritime convection observed during AMMA/NAMMA; *Quart. J. Roy. Meteor. Soc.* **137** 1241–1256.

Halverson J B, Rickenbach T, Roy B, Pierce H and Williams E 2002 Environmental characteristics of convective systems during TRMM-LBA; *Mon. Wea. Rev.* **130** 1493–1509.

Helms C N and Hart R E 2015 The evolution of dropsonde-derived kinematic and thermodynamic structures in developing and non-developing Atlantic tropical convective systems; *Mon. Wea. Rev.* **143** 3109–3135.

Houze R A and Cheng C-P 1977 Radar characteristics of tropical convection observed during GATE: Mean properties and trends over the summer season; *Mon. Wea. Rev.* **105** 964–980.

Houze RA 1979 Cloud and precipitation structure of mesoscale systems in GATE. Proceedings, Impact of GATE on Large-scale Numerical Modeling of the Atmosphere and Ocean; Woods Hole, *National Academy of Sciences,* pp. 100–108.

Houze R A and Betts A K 1981 Convection in GATE; *Rev. Geophys.* **19** 541–576.

Houze R A 1982 Cloud clusters and large-scale vertical motions in the tropics; *J. Meteor. Soc. Japan* **60** 39—410.

Houze Jr RA 1989 Observed structure of mesoscale convective systems and implications for large-scale heating; *Quart. J. Roy. Meteor. Soc.* **115** 425–461.

Houze R A, Rutledge S A, Biggerstaff M I and Smull B F 1989 Interpretation of Doppler weather radar displays in mid-latitude mesoscale convective systems; *Bull. Amer. Meteor. Soc.* **70** 608–619.

Houze R A 1993 *Cloud Dynamics*; Academic Press, 573p.

Houze Jr R A 2004 Mesoscale convective systems; *Rev. Geophys.* **42** RG4003.

Hubbert J C, Dixon M, Ellis S M and Meymaris G 2009 Weather radarground clutter. Part I: Identification, modeling, and simulation; *J. Atmos. Oceanic. Technol.* **26** 1165–1180.

Jabouille P, Redelsperger J L and Lafore J P 1996 Modification of surface fluxes by atmospheric convection in the TOGA COARE region; *Mon. Wea. Rev.* **124** 816–837.

Johnson R H and Nicholls M 1983 A compositive analysis of the boundary layer accompanying a tropical squall line; *Mon. Wea. Rev.* **111** 308–319.

Johnson R H and Hamilton P J 1988 The relationship of surface pressure features to the precipitation and airflow structure of an intense midlatitude squall line; *Mon. Wea. Rev.* **116** 1444–1473.

Johns R H and Doswell III C A 1992 Severe local storms forecasting; *Wea. Forecasting* **7** 588–612.

Jorgensen D P, LeMone M A and Trier SB 1997 Structure and evolution of the 22 February 1993 TOGA COARE squall line: Aircraft observations of precipitation, circulation, and surface energy fluxes; *J. Atmos. Sci.* **54** 1961–1985.

Joseph P V 2009 Local severe storms; *Mausam* **60** 139–154.

Kim H W and Lee D K 2006 An observational study of mesoscale convective systems with heavy rainfall over the Korean peninsula; *Wea. Forecasting* **21** 125–148.

Knupp K, Ware R, Cimni D, Vandenberghe F, Vivekanandan J, Westwater E and Coleman T 2009 Ground-based passive microwave profiling during dynamic weather conditions; *J. Atmos. Oceanic Technol.* **26** 1057–1072.

Kumar K K, Jain A R and Narayana Rao D 2005 VHF/UHF radar observations of tropical mesoscale convective systems over southern India; *Ann. Geophys.* **23** 1673–1683.

Lagouvardos K, Kotroni V, Defer E and Bousquet O 2013 Study of a heavy precipitation event over southern France, in the frame of HYMEX project: Observational analysis and model results using assimilation of lightning; *Atmos. Res.* **134** 45–55.

Lang T J, Miller L J, Weisman M and Rutledge S A 2004 The severe thunderstorm electrification and precipitation study; *Bull. Am. Meteor. Soc.* **5** 1107.

Latha R and Murthy B S 2011 Boundary layer signatures of consecutive thunderstorms as observed by Doppler sodar over western India; *Atmos. Res.* **99** 230–240.

Laurent H, Machado L A, Morales C A and Durieux L 2002 Characteristics of the Amazonian mesoscale convective systems observed from satellite and radar during the WETAMC/LBA experiment; *J. Geophys. Res.* **107(D20)** 8054, https://doi.org/10.1029/2001jd000337.

Leary C A and Houze Jr R A 1979 The structure and evolution of convection in a tropical cloud cluster; *J. Atmos. Sci.* **36** 437–457.

Lee K O, Flamant C, Ducrocq V, Duffourg F, Fourrié N and Davolio S 2016 Convective initiation and maintenance processes of two back-building mesoscale convective systems leading to heavy precipitation events in Southern Italy during HyMeX IOP 13; *Quart. J. Roy. Meteor. Soc.* **142** 2623–2635.

LeMone M A, Zipser E J and Trier S B 1998 The role of environmental shear and thermodynamic conditions in determining the structure and evolution of mesoscale convective systems during TOGA COARE; *J. Atmos. Sci.* **55** 3493–3518.

Litta A J, Mohanty U C, Das S and Idicula S M 2012 Numerical simulation of severe local storms over east India using WRF-NMM mesoscale model; *Atmos. Res.* **116** 161–184.

Maddox R A 1980 Mesoscale convective complexes; *Bull. Am. Meteor. Soc.* **61** 1374–1387.

Madhulatha A, George J P and Rajagopal E N 2017 All-sky radiance simulation of Megha-Tropiques SAPHIR microwave sensor using multiple scattering radiative transfer model for data assimilation applications; *J. Earth. Sys. Sci.* **126** 24.

Madhulatha A, Rajeevan M, Venkat Ratnam, M, Bhate J and Naidu CV 2013 Nowcasting severe convective activity over southeast India using ground-based microwave radiometer observations; *J. Geophys. Res. Atmos.* **118** 1–13.

Madhulatha A and Rajeevan M 2018 Impact of different parameterization schemes on simulation of mesoscale convective system over south-east India; *Meteor. Atmos. Phys.* **130** 49–65.

Madhulatha A, Rajeevan M, Bhowmik S R and Das A K 2018 Impact of assimilation of conventional and satellite radiance GTS observations on simulation of mesoscale convective system over southeast India using WRF-3DVar; *Pure Appl. Geophys.* **175** 479–500.

Mapes E B, Warner T T and Xu M 2003 Diurnal patterns of rainfall in northwestern South America. Part 3: Diurnal gravity waves and nocturnal convection offshore; *Mon. Wea. Rev.* **131** 830–844.

Marsham J H, Trier S B, Weckwerth T M and Wilson J W **2011** Observations of elevated convection initiation leading to a surface-based squall line during 13 June IHOP_2002; *Mon. Wea. Rev.* **139** 247–271.

Moncrieff MW 2010 The multiscale organization of moist convection at the intersection of weather and climate. Why does climate vary? Geophys. Monogr., Vol. 189, *Am. Geophys. Union,* pp. 3–26.

Moore T J, Glass F H, Graves C E, Rochette S M and Singer M J 2003 The environment of warm season elevated thunderstorms associated with heavy rainfall over the central United States; *Wea. Forecasting* **18** 861–878.

Moore J T 1987 Isentropic analysis and interpretation: Operational applications to synoptic and mesoscale forecast problem, Air Weather Service Tech. Note. AWS-TN-87-002, 85p. [Available from USAF, ETAC, Scott Air Force Base, IL 62225-5458].

Mukhopadhyay P, Singh H A K and Singh S S 2005 Two severe Nor'westers in April 2003 over Kolkata, India using Doppler radar observations and satellite imageries; *Weather* **60** 343–353.

Parker M D and Johnson R H 2004 Structures and dynamics of quasi-2D mesoscale convective systems; *J. Atmos. Sci.* **61** 545–567.

Peterson W A and Rutledge S A 1998 On the relationship between cloud-to-ground lightning and convective rainfall; *J. Geophys. Res. Atmos.* **103** 14,025–14,040.

Parsons D, Dabberdt W, Cole H, Hock T, Martin C, Barrett A L, Miller E, Spowart M, Howard M, Ecklund W and Carter D 1994 The integrated sounding system: Description and preliminary observations from TOGA COARE; *Bull. Am. Meteor. Soc.* **75** 553–567.

Raghavan S 2013 *Radar meteorology* (Vol. 27); Springer Science & Business Media.

Rajesh Rao P, Kalyana Sundaram S, Thampi S B, Suresh R and Gupta J P 2004 An overview of first Doppler Weather Radar inducted in the cyclone detection network of India Meteorological Department; *Mausam* **55** 155–176.

Rajeevan M, Kesarkar A, Thampi S B, Rao T N, Radhakrishna B and Rajasekhar M 2010 Sensitivity of WRF cloud microphysics to simulations of a severe thunderstorm event over southeast India; *Ann. Geophys.* **28** 603–619.

Ramis C, Romero R and Homar V 2009 The severe thunderstorm of 4 October 2007 in Mallorca: An observational study; *Nat. Hazards Earth Syst. Sci.* **9** 1237–1245, https://doi.org/10.5194/nhess-9-1237-2009.

Rao P B, Jain A R, Kishore P, Balamuralidhar P and Damle S H 1995 1. System description and sample vector wind measurements; *Radio. Sci.* **30** 1125–1138.

Rasmussen K L and Houze Jr R A 2011 Orogenic convection in South America as seen by the TRMM satellite; *Mon. Wea. Rev.* **139** 2399–2420.

Ratnam M V, Santhi Y D, Rajeevan M and Rao S V B 2013 Diurnal variability of stability indices observed using radiosonde observations over a tropical station: Comparison with microwave radiometer measurements; *Atmos. Res.* **124** 21–33.

Rienecker M M, Suarez M J, Gelaro R, Todling R, Bacmeister J, Liu E, Bosilovich E G, Schubert S D, Takacs L, Kim G K, Bloom S, Chen J, Collins D, Conaty A, da Silva A et al 2011 MERRA: NASA's Modern-Era Retrospective Analysis for Research and Applications; *J. Climat.* **24** 3624–3648. https://doi.org/10.1175/JCLI-D-11-00015.1.

Rutledge S A and MacGorman D R 1988 Cloud-to-ground lightning activity in the 10–11 June 1985 mesoscale convective system observed during the Oklahoma–Kansas PRE-STORM project; *Mon. Wea. Rev.* **116** 1393–1408.

Rutledge S A, Houze R A, Heymsfield A J and Biggerstaff M I 1988 Dual-Doppler and airborne microphysical observations in the stratiform region of the 10–11 June MCS over Kansas during PRE-STORM. Preprints, 10th Int. Cloud Physics Conf, Bad Homburg, Germany, Deutscher Wetterdienst, pp. 702–704.

Shaw N and Austin E 1930 *Manual of meteorology*; vol. 3: the physical processes of weather.

Srinivasulu P, Yasodha P, Kamaraj P, Rao T N, Jayaraman A, Reddy S N and Satyanarayana S 2012 1280-MHz active array radar wind profiler for lower atmosphere: System description and data validation; *J. Atmos. Oceanic Technol.* **29** 1455–1470.

Thapliyal P K, Shukla M V, Shah S, Joshi P C, Pal P K and Ajil K S 2011 An algorithm for the estimation of upper tropospheric humidity from Kalpana observations: Methodology and validation; *J. Geophys. Res.* **116** D01108, https://doi.org/10.1029/2010jd014291.

Tyagi A, Sikka D R, Goyal S and Bhowmick M 2012 A satellite-based study of pre-monsoon thunderstorms (nor'westers) over eastern India and their organization into mesoscale convective complexes; *Mausam* **63** 29–54.

Tyagi B, Satyanarayana A N V and Naresh Krishna V 2013 Thermodynamical structure of atmosphere during pre-monsoon thunderstorm season over Kharagpur as revealed by STORM data; *Pure Appl. Geophys.* **170** 675–687, https://doi.org/10.1007/s00024-012-0566-5.

Wang J J 2004 Evolution and structure of the mesoscale convection and its environment: A case study during the early onset of the southeast Asian summer monsoon; *Mon. Wea. Rev.* **132** 1104–1120.

Wapler K and James P 2015 Thunderstorm occurrence and characteristics in Central Europe under different synoptic conditions; *Atmos. Res.* **158** 231–244.

Ware R, Cimini D, Campos E, Giuliani G, Albers S, Nelson M, Koch K E,Joe P and Cober S 2013 Thermodynamic and liquid profiling during the 2010 Winter Olympics; *Atmos. Res.* **132–133** 278–290. https://doi.org/10.1016/j.atmosres.2013.05.019.

Weckwerth T M, Murphey H V, Flamant C, Goldstein J and Pettet C R 2008 An observational study of convection initiation on 12 June 2002 during IHOP_2002; *Mon. Wea. Rev.* **136** 2283–2300.

Wilson J W, Crook N A, Mueller C K, Sun J and Dixon M 1998 Nowcasting thunderstorms: A status report; *Bull. Am. Meteor. Soc.* **79** 2079–2099.

Williams C R 2012 Vertical air motion retrieved from dual-frequency profiler observations; *J. Atmos. Oceanic Technol.* **29** 1471–1480.

Yuter S E and Houze Jr R A 1998 The natural variability of precipitating clouds over the western Pacific warm pool; *Quart. J. Roy. Meteor. Soc.* **124** 53–99.

Zhang C and Yoneyama K 2017 CINDY/DYNAMO field campaign: Advancing our understanding of MJO initiation; In: The global monsoon system, *Research and Forecast,* pp. 339–348.

Zhong L, Mu R, Zhang D, Zhao P, Zhang Z and Wang N 2015 An observational analysis of warm-sector rainfall characteristics associated with the 21 July 2012 Beijing extreme rainfall event; *J. Geophys. Res. Atmos.* **120** 3274–3291.

Zuluaga M D and Houze Jr RA 2013 Evolution of the population of precipitating convective systems over the equatorial Indian Ocean in active phases of the Madden–Julian oscillation; *J. Atmos. Sci.* **70** 2713–2725, https://doi.org/10.1175/jas-d-12-0311.1.

Corresponding editor: N V Chalapathi Rao